Bioorganic Chemistry 111 (2021) 104847

Contents lists available at ScienceDirect

Bioorganic Chemistry

journal homepage: www.elsevier.com/locate/bioorg

α-Glucosidase inhibitory and anti-inflammatory activities of dammarane triterpenoids from the leaves of *Cyclocarya paliurus*

Chenguo Li [a], Shengping Deng [a], Wei Liu [a], Dexiong Zhou [a], Yan Huang [a], Cheng-qin Liang [c], Lili Hao [a], Gaorong Zhang [a], Shanshan Su [a], Xia Xu [a], Ruiyun Yang [a], Jun Li [a,b,*], Xishan Huang [a,*]

[a] State Key Laboratory for Chemistry and Molecular Engineering of Medicinal Resources, Collaborative Innovation Center for Guangxi Ethnic Medicine, School of Chemistry and Pharmaceutical Science, Guangxi Normal University, Guilin 541004, China
[b] Institute for Sustainable Development and Innovation, Guangxi Normal University, Guilin 541004, China
[c] College of Pharmacy, Guilin Medical University, Guilin 541004, China

ARTICLE INFO

Keywords:
Cyclocarya paliurus
Diabetes
α-glucosidase
Anti-inflammatory
Triterpenoid

ABSTRACT

Diabetes mellitus is caused by chronic inflammation and affects millions of people worldwide. *Cyclocarya paliurus* leaves have been widely used in traditional folk tea as a remedy for diabetes, but the antidiabetic constituents remain to be further studied. The α-glucosidase inhibitory and anti-inflammatory activities were examined to evaluate their effects on diabetes mellitus, and bioassay-guided separation of *C. paliurus* leaves led to the identification of twenty dammarane saponins, including eleven new dammarane saponins (**1**–**11**). The structures of the isolates were elucidated by spectroscopic methods. Bioactivity assay results showed that compounds **1** and **2** strongly inhibited α-glucosidase activity, with IC_{50} values ranging from 257.74 μM, 282.23 μM, and strongly inhibited the release of NO, with IC_{50} values of 9.10 μM, 9.02 μM. Moreover, compound **2** significantly down-regulated the mRNA expression of iNOS, COX-2, IL-1β, NF-κB, IL-6 and TNF-α in LPS-mediated RAW 264.7 cells and markedly suppressed the protein expression of iNOS, NF-κB/p65, and COX-2. Dammarane glucoside **2** exhibited the strongest α-glucosidase inhibitory and anti-inflammatory activities. In addition, the structure–activity relationships (SARs) of the dammarane saponins were investigated. In summary, *C. paliurus* leaves showed marked α-glucosidase inhibitory and anti-inflammatory activities, and dammarane saponins are responsible for regulating α-glucosidase, inflammatory mediators, and mRNA and the protein expression of proinflammatory cytokines, which could be meaningful for discovering new antidiabetic agents.

1. Introduction

In recent years, with an increase in the intake of high-energy-content foods, nutritional balance has been overlooked, and the incidence of diabetes is increasing at an alarming rate [1]. Diabetes is associated with a high-carbohydrate diet, and starches are one of the main sources of carbohydrates. Inhibiting carbohydrate digestive enzymes by delaying glucose absorption is one of the most effective ways of overcoming postprandial hyperglycemia [2]. α-Glucosidase, a carbohydrate digestive enzyme, is an essential target for the regulation of postprandial serum glucose in diabetic patients [3,4]. Additionally, inflammation plays a significant role in the progression of diabetes. Higher concentrations of inflammatory mediators, such as nitric oxide (NO), and proinflammatory cytokines, such as interleukin-1β (IL-1β), interleukin-6 (IL-6), cyclooxygenase-2 (COX-2), inducible nitric oxide synthase (iNOS), nuclear factor kappa-B (NF-κB/p65), and tumor necrosis factor-alpha (TNF-α) are present in diabetic patients than in healthy patients [5,6]. These proinflammatory cytokines cause damage in pancreatic

Abbreviations: PNPG, 4-nitrophenyl-α-D-glucopyranoside; IL-1β, interleukin-1β; IL-6, interleukin-6; COX-2, cyclooxygenase-2; iNOS, inducible nitric-oxide synthase; NF-κB/p65, nuclear factor kappa-B; mRNA, messenger RNA; cDNA, complementary DNA; HRESIMS, high resolution electrospray ionization mass spectroscopy; NMR, nuclear magnetic resonance; HMBC, heteronuclear multiple-bond correlation; H–H COSY, H–H correlated spectroscopy; ROESY, rotating frame Overhauser effect spectroscopy; DMEM, Dulbecco's modified eagle medium; SDS-PAGE, sodium dodecyl sulfate polyacrylamide gel electrophoresis; SPR, surface plasmon resonance; MTT, 3-(4,5-dimethylthiazol-2yl)-2,5-diphenyltetrazolium bromide; PVDF, poly (vinylidene difluoride).

* Corresponding authors at: State Key Laboratory for Chemistry and Molecular Engineering of Medicinal Resources, Collaborative Innovation Center for Guangxi Ethnic Medicine, School of Chemistry and Pharmaceutical Science, Guangxi Normal University, Guilin 541004, China.
E-mail addresses: lijun9593@gxnu.edu.cn (J. Li), huangxishan13@foxmail.com (X. Huang).

https://doi.org/10.1016/j.bioorg.2021.104847
Received 5 August 2020; Received in revised form 14 January 2021; Accepted 18 March 2021
Available online 22 March 2021

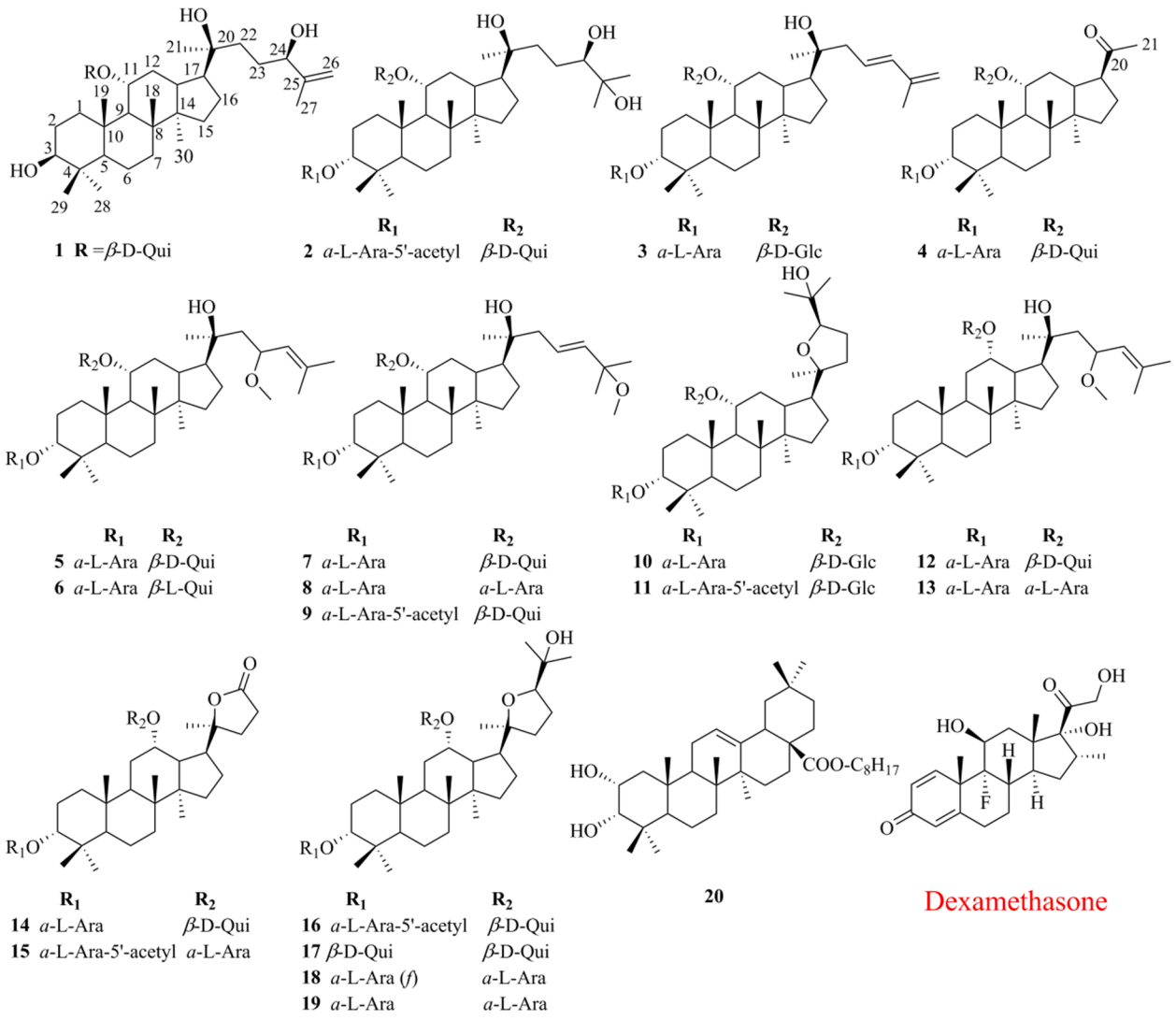

Fig. 1. Structures of compunds **1**–**20** isolated from *C. paliurus*.

tissue, adipose tissue and the vasculature. In particular, NF-κB plays an important role in initiating the inflammatory response during the production of proinflammatory cytokines and to the mRNA expression and protein expression of iNOS, COX-2, IL-1β, NF-κB, IL-6 and TNF-α [7,8]. Activation of the NF-κB signaling pathway and excessive amounts of inflammatory cytokines are considered to be possible mechanisms that lead to diabetic diseases [9,10].

Cyclocarya paliurus, an endemic species that grows in southern China, has been widely used as a traditional sweet tea to prevent diabetes, inflammation, hypertension, and heart disease and as a traditional medicine for the treatment of diabetes mellitus, chronic inflammatory diseases, hyperlipidemia, and hypertension [11,12]. Dammarane triterpenoids, of which compounds were firstly isolated in 1992 [13,14], are considered characteristic indicators of the plant and the key functional and active constituents of *C. paliurus*. The extract of *C. paliurus* leaves has shown significant antidiabetic effects in many reports [15–21]. The *C. paliurus* antidiabetic prescription reduces blood glucose and improves glucose tolerance [22,23]. The *C. paliurus* antidiabetic mechanism may be related to antioxidative and anti-inflammatory effects [12]. However, the possible antidiabetic compounds in *C. paliurus* leaves and their corresponding mechanisms remain unclear.

To further investigate potential constituents to treat diabetes based on α-glucosidase inhibitory and anti-inflammatory activities, the *p*-nitrophenol-α-D-glucopyranoside (PNPG) method and RAW 264.7 cells were used as bioassay-guided evaluation models to verify the antidiabetic effects of *C. paliurus* leaves and identify the active constituents. The active portion was separated to obtain twenty dammarane saponins (**1**–**20**), including eleven new dammarane saponins (**1**–**11**) (Fig. 1). Furthermore, the inhibition of α-glucosidase and NO by the extracts and the isolates was evaluated. In addition, the effects of the most active anti-inflammatory compound on the mRNA expression of the inflammatory cytokines iNOS, NF-κB, COX-2, IL-6, IL-1β and TNF-α and the protein expression of iNOS, COX-2 and NF-κB/p65 were tested using LPS-mediated RAW 264.7 macrophages. Herein, the isolation, purification and determination of these isolates, the assays used to determine the antidiabetic and anti-inflammatory activities of the constituents, the effects of the most active compound on mRNA and the protein expression of some inflammatory cytokines, and the structure–activity relationships (SARs) are described.

2. Materials and methods

2.1. General experimental procedures

Silica gel (100–200 mesh, Qingdao Marine Chemical Co. Ltd.), reversed-phase C_{18} (50 μm, Merck), and Sephadex LH-20 (Amersham Pharmacia Biotech) columns were used for chromatographic separations. L-Arabinose, D-arabinose, L-glucose, D-glucose, L-quinovose and D-

Table 1
^{1}H NMR Spectral Data of Compounds 1–6 (500 MHz and 600 MHz, Pyridine-d_5, δ in ppm).

position	Compound **1** δ_H, mult (*J* in Hz)[a]	Compound **2** δ_H, mult (*J* in Hz)[b]	Compound **3** δ_H, mult (*J* in Hz)[a]	Compound **4** δ_H, mult (*J* in Hz)[a]	Compound **5** δ_H, mult (*J* in Hz)[b]	Compound **6** δ_H, mult (*J* in Hz)[b]
1	3.08, td, (9.9, 2.7); 2.12, m	2.99, m; 1.80, m	3.04, m; 1.84, m	3.01, m; 1.83, m	3.02, m; 1.83, m	3.06, td, (9.0, 3.8); 1.83, m
2	2.16, m; 1.75, m	1.79, m; 1.65, m	1.75, m; 1.66, m	1.81, m; 1.69, m	1.81, m; 1.70, m	1.73, m; 1.61, m
3	3.62, m	3.54, m	3.56, m	3.61, br s	3.60, m	3.55, m
5	1.80, m	1.54, m	1.55, m	1.55, m	1.56, m	1.55, m
6	1.54, m; 1.47, m	1.53, m; 1.47, m	1.54, m; 1.45, m	1.47, m; 1.41, m	1.48, m; 1.45, m	1.48, m; 1.46, m
7	1.63, m; 1.22, dt, (13.0, 3.0)	1.53, m; 1.19, m	1.52, m; 1.16, m	1.52, m; 1.12, overlapped	1.54, m; 1.18, overlapped	1.53, m; 1.16, m
9	2.04, m	1.88, m	1.90, m	1.85, m	1.90, m	1.90, m
11	4.48, td, (10.5, 5.0)	4.45, td, (10.6, 4.9)	4.51, m	4.46, dt, (10.6, 5.4)	4.47, td, (10.6, 4.9)	4.48, td, (10.8, 5.1)
12	2.95, m; 1.71, m	2.97, m; 1.59, m	2.99, m; 1.68, m	2.58, m; 1.55, m	2.99, t (4.5); 1.67, m	3.04, t (3.9); 1.66, m
13	2.16, m	2.02, dd, (10.2, 2.5)	2.12, m	2.21, m	2.12, m	2.12, m
15	1.53, m; 1.06, t (10.4)	1.42, m; 1.01, dt, (11.0, 7.6)	1.50, m; 1.03, t, (9.5)	1.48, m; 1.05, m	1.48, m; 1.03, dt, (12.5, 8.2)	1.48, m, 1.04, t, (8.6)
16	2.14, m; 1.74, m	1.75, m; 1.44, m	1.88, m; 1.80, m	1.90, m; 1.70, m	1.75, m; 1.45, m	1.73, m; 1.45, m
17	1.80, m	1.89, m	1.96, m	2.55, m	1.85, m	1.86, m
18	1.11, s	1.08, s	1.00, s	1.02, s	1.07, s	1.03, s
19	1.40, s	1.33, s	1.33, s	1.34, s	1.35, s	1.32, s
21	1.44, s	1.25, s	1.42, s	2.07, s	1.43, s	1.47, s
22	2.12, m; 1.96, m	2.29, td, (12.5, 4.0); 1.75, m	2.65, dd, (13.5, 6.6); 2.50, m		2.14, m; 1.67, m	2.18, m; 1.66, m
23	2.10, m; 2.02, m	1.90, m; 1.78, m	6.11, d, (7.7)		4.39, m	4.42, td, (9.0, 4.5)
24	4.42, m	3.68, d	6.41, d, (15.5)		5.15, dt, (9.0, 1.3)	5.21, m
26	5.30, s; 4.98, s	1.50, s	5.05, s, 4.94, s		1.69, s	1.72, s
27	1.91, s	1.29, s	1.83, s		1.68, s	1.71, s
28	1.00, s	0.93, s	0.88, s	0.95, s	0.95, s	0.91, s
29	1.26, s	1.24, s	1.25, s	1.29, s	1.28, s	1.25, s
30	0.87, s	0.76, s	0.76, s	0.70, s	0.79, s	0.77, s
1′		5.49, m	5.52, br s	5.56, br s	5.54, d, (1.3)	5.49, m
2′		4.84, d, (2.8)	4.86, m	4.87, m	4.86, m	4.84, m
3′		4.61, d, (3.4)	4.82, m	4.84, m	4.82, m	4.83, m
4′		4.72, td, (6.9, 3.1)	4.73, m	4.75, m	4.72, d, (3.4)	4.71, m
5′		4.79, dd, (11.6, 3.0); 4.59, m	4.38, m; 4.27, d, (4.6)	4.39, m; 4.28, dd, (11.7, 4.4)	4.36, m; 4.26, dd, (11.9, 4.8)	4.35, m; 4.26, m
1″	4.93, d, (7.6)	5.03, d, (7.7)	5.06, br s	4.87, dd, (15.9)	4.95, d, (7.7)	4.81, d, (3.9)
2″	3.98, t, (8.3)	3.94, t, (8.4)	3.98, t, (8.2)	3.94, t, (8.4)	3.95, t, (8.5)	4.34, d, (7.4)
3″	4.10, t, (8.7)	4.13, t, (8.8)	4.20, t, (8.5)	4.11, t, (8.8)	4.09, t, (8.8)	4.05, dd, (9.2, 3.7)
4″	3.66, t, (8.8)	3.68, d, (8.9)	3.87, m	3.69, t, (8.9)	3.66, t, (8.8)	4.20, m
5″	3.60, d, (5.9)	3.74, m	4.12, t, (8.8)	3.63, m	3.63, m	4.28, dd, (10.3, 2.2); 3.62, m
6″	1.61, d, (5.8)	1.55, d, (5.9)	4.52, dd, (11.2, 2.8); 4.33, dd, (11.2, 5.3)	1.62, d, (5.9)	1.60, d, (5.9)	
CH_3COO—						
CH_3COO—		1.96, s				
—OCH_3					3.19, s	3.21, s

[a] Recorded at 600 MHz for ^{1}H NMR in pyridine-d_5, *J* values (Hz) were determined from ^{1}H- decoupling experiments.
[b] Recorded at 500 MHz for ^{1}H NMR in pyridine-d_5, *J* values (Hz) were determined from ^{1}H- decoupling experiments.

quinovose were used as sugar standards (Sigma, Munich, Germany). All solvents were of HPLC or analytical grade. The instruments used in the experiment are shown in the Supporting Information (SI, Text S1).

2.2. Plant material

Dried leaves (10 kg) of *C. paliurus* were obtained from Xiushui County, Jiangxi, China, in July 2017 and identified by Associate Professor Qiang Xie (Guangxi Normal University). A voucher specimen (No. ID-20170705) was deposited at the State Key Laboratory of Guangxi Normal University (GXNU), China.

2.3. Extraction and bioactivity-guided separation of dammarane saponins

The leaves of *C. paliurus* (sweet tea, 10 kg) were extracted 3 times with a 75% ethanol-H_2O mixture (3:1, v/v, 20 L) under reflux and concentrated under vacuum to remove the ethanol. The remaining H_2O portion was further subjected to macroporous resin column chromatography (D101, H_2O/MeOH 10:30 → 10:90, 10000 mL each) to provide six fractions. The α-glucosidase inhibitory activity was tested by the PNPG method, and the anti-inflammatory effects were assayed by measuring the inhibition degree of NO production in LPS-mediated RAW 264.7 cells.

The active fraction (300 g) was chromatographed on a silica gel column eluted with a gradient of increasing methanol amounts (0 → 100%) in a mixture with dichloromethane to yield 8 fractions (Fr.I to Fr. VIII). Fr.V (40 g) with active α-glucosidase inhibitory and anti-inflammatory activities was subjected to MCI gel column chromatography (CHP20P, MeOH/H_2O 50:50 → 90:10, 1000 mL each) to provide six fractions (Fr.V-1 to Fr. −6). Fr.V-3 (10 g) was fractioned by an ODS column (MeOH-H_2O, 60:40 → 100:0) to obtain six subfractions (Fr.V-3-1 to Fr.V-3-6). Fr.V-3-2 (800 mg) was isolated with a Sephadex LH-20 column, which was followed by semipreparative HPLC (MeCN-H_2O, 50:50, v/v, 3.0 mL/min, λ = 205 nm) to yield **2** (t_R 13.86 min, 10.7 mg), **4** (t_R 19.12 min, 6.2 mg), **10** (t_R 15.17 min, 7.1 mg), **12** (t_R 23.16 min, 4.0 mg), and **13** (t_R 22.06 min, 5.8 mg). Fr.V-3-3 was purified by preparative MPLC (MeCN-H_2O, 50:50, v/v, 8.0 mL/min, λ = 205 nm) and semipreparative HPLC (MeOH-H_2O, 78:22, v/v, 3.0 mL/min, λ = 205 nm) to obtain **5** (t_R 16.98 min, 6.2 mg), **6** (t_R 16.16 min, 5.0 mg), **9** (t_R 16.53 min, 4.7 mg), **11** (t_R 16.04 min, 7.5 mg), and **14** (t_R 27.44 min, 8.1 mg). Compounds **7** (t_R 14.16 min, 6.6 mg), **8** (t_R 17.98 min, 4.1 mg), and **15** (t_R 35.41 min, 4.7 mg) were isolated from Fr.V-3-4 using preparative

Table 2
^{1}H NMR Spectral Data of Compounds 7–10 (500 MHz and 600 MHz, Pyridine-d_5, δ in ppm).

position	Compound **7** δ_H, mult (*J* in Hz)[a]	Compound **8** δ_H, mult (*J* in Hz)[b]	Compound **9** δ_H, mult (*J* in Hz)[b]	Compound **10** δ_H, mult (*J* in Hz)[a]	Compound **11** δ_H, mult (*J* in Hz)[a]
1	3.03, td, (10.8, 3.5); 1.84, m	3.07, m; 1.83, m	3.02, td, (8.71, 4.5); 1.82, m	3.06, m; 1.85, m	3.06, m; 1.83, m
2	1.83, m, 1.70, m	1.82, m; 1.70, m	1.80, m; 1.69, m	1.74, m; 1.67, m	1.74, m; 1.64, m
3	3.61, m	3.55, m	3.57, m	3.58, br s	3.54, br s
5	1.56, m	1.54, m	1.56, m	1.56, m	1.55, m
6	1.50, m; 1.47, m	1.51, m; 1.44, m	1.50, m; 1.47, m	1.55, m; 1.44, m	1.53 m; 1.40, m
7	1.58, m; 1.21, dt, (13.0, 3.0)	1.55, m; 1.18, overlapped	1.57, m; 1.21, dt, (13.0, 3.0)	1.52, m; 1.15, m	1.51, m; 1.17, d, (12.4)
9	1.90, m	1.90, m	1.90, m	1.89, m	1.88, m
11	4.47, td, (10.6, 4.9)	4.47, td, (10.6, 5.0)	4.47, td, (10.8, 4.5)	4.48, td, (10.5, 5.0)	4.48, m
12	2.98, m; 1.67, m	3.02, m; 1.67, m	2.98, m; 1.67, m	2.97, d, (12.5); 1.57, m	2.97, d, (12.3); 1.59, m
13	2.18, m	2.17, m	2.17, m	1.81, m	1.81, m
15	1.55, m; 1.07, t, (10.6)	1.53, m; 1.08, t, (9.3)	1.55, m; 1.06, t, (10.1)	1.39, m; 0.99, t, (9.9)	1.39, m; 1.00, t, (9.3)
16	1.92, m, 1.84, m	1.90, m; 1.83, m	1.91, m; 1.83, m	1.77, m; 1.45, m	1.79, m; 1.43, m
17	1.96, m	1.96, m	1.95, m	1.90, m	1.90, m
18	1.09, s	1.05, s	1.09, s	1.02, s	1.02, s
19	1.35, s	1.32, s	1.34, s	1.36, s	1.35, s
21	1.44, s	1.47, s	1.44, s	1.18, s	1.19, s
22	2.61, dd, (13.5, 6.2); 2.43, dd, (13.5, 8.7)	2.62, dd, (13.6, 6.0); 2.46, dd, (13.6, 8.6)	2.61, dd, (13.4, 6.2); 2.43, dd, (13.4, 8.5)	1.75, m; 1.56, m	1.77, m; 1.57, m
23	5.98, ddd, (15.8, 8.7, 6.2)	6.00, ddd, (15.9, 8.6, 6.0)	5.97, ddd, (15.9, 8.5, 6.2)	2.04, m; 1.95, m	2.03, m; 1.95, m
24	5.65, d, (15.8)	5.67, d, (15.9)	5.64, d, (15.9)	3.96, m	3.96, t
26	1.31, s	1.31, s	1.30, s	1.47, s	1.48, s
27	1.31, s	1.31, s	1.30, s	1.41, s	1.42, s
28	0.96, s	0.90, s	0.96, s	0.89, s	0.90, s
29	1.29, s	1.26, s	1.26, s	1.27, s	1.27, s
30	0.80, s	0.78, s	0.81, s	0.72, s	0.73, s
1′	5.51, br s	5.48, br s	5.51, br s	5.53, br s	5.50, br s
2′	4.88, m	4.84, m	4.86, m	4.87, m	4.87, m
3′	4.84, m	4.81, m	4.63, m	4.83, m	4.63, dt
4′	4.75, m	4.72, ddd, (6.3, 4.7, 3.5)	4.73, m	4.74, m	4.74, td, (5.7)
5′	4.38, m; 4.28, dd, (11.8, 4.6)	4.34, m; 4.25, dd, (11.5, 4.7)	4.81, dd, (11.6, 3.0); 4.62, m	4.37, m; 4.28, m	4.81, d, (11.5, 3.0);4.61, m
1″	4.94, d, (7.7)	4.83, br s	4.93, d, (7.7)	5.16, d, (7.7)	5.16, d, (7.7)
2″	3.96, t, (8.3)	4.36, m	3.94, m	4.00, d, (8.3)	3.99, t, (8.3)
3″	4.11, t, (8.8)	4.06, dd, (9.2, 3.6)	4.09, t, (8.7)	4.29, m	4.30, t, (8.8)
4″	3.69, t, (8.9)	4.21, m	3.69, m	4.03, dd, (8.1, 4.2)	4.03, m
5″	3.64, m	4.30, m; 3.64, m	3.64, m	4.17, t, (9.0)	4.17, t, (9.1)
6″	1.62, d, (5.8)		1.61, d, (5.8)	4.54, d, (11.1); 4.39, m	4.54, d; 4.36, d, (10.6)
—OCH_3	3.20, s	3.21, s	3.20, s		
CH_3COO—			1.97, s		1.97, s

[a] Recorded at 600 MHz for ^{1}H NMR in pyridine-d_5, *J* values (Hz) were determined from ^{1}H- decoupling experiments.
[b] Recorded at 500 MHz for ^{1}H NMR in pyridine-d_5, *J* values (Hz) were determined from ^{1}H- decoupling experiments.

MPLC (MeCN-H_2O, 50:50, v/v, 8.0 mL/min, λ = 210 nm) and semi-preparative HPLC (MeOH-H_2O, 78:22, v/v, 3.0 mL/min, λ = 210 nm). Fr.V-3-5 was chromatographed on a silica gel column by eluting with CH_2Cl_2-MeOH and purified by preparative MPLC (C_2H_3N-H_2O, 55:45, v/v, 8.0 mL/min, λ = 205 nm) and semipreparative HPLC (MeOH-H_2O, 80:20, v/v, 3.0 mL/min, λ = 205 nm) to obtain **1** (t_R 33.18 min, 14.3 mg), **3** (t_R 16.83 min, 7.4 mg), and **16** (t_R 21.44 min, 9.0 mg). Fr.V-4 was fractioned with an ODS column (MeOH-H_2O, 50:50 → 100:0) to obtain five subfractions (Fr.V-4-1 to Fr.V-45). Fr.V-4-4 was purified by preparative MPLC (MeCN-H_2O, 50:50, v/v, 8.0 mL/min, λ = 205 nm) and semipreparative HPLC (MeOH-H_2O, 80:20, v/v, 3.0 mL/min, λ = 205 nm) to give **17** (t_R 14.16 min, 6.0 mg), **18** (t_R 17.53 min, 5.2 mg), **19** (t_R 15.08 min, 3.7 mg), and **20** (t_R 40.15 min, 4.4 mg).

2.3.1. *Cyclocarioside Z_9* ***(1)***

The chromatographic separation and purification method afforded 14.3 mg of a white amorphous powder; $[\alpha]_D^{25}$ + 1.10 (*c* 0.17, MeOH); HRESIMS *m/z* 645.4342 $[M+Na]^+$ (calculated for $C_{36}H_{62}O_8Na$, 645.4341); for the ^{1}H (pyridine-d_5, 600 MHz) and ^{13}C NMR (pyridine-d_5, 150 MHz) data, see Tables 1 and 3.

2.3.2. *Cyclocarioside Z_{10}* ***(2)***

The chromatographic separation and purification method afforded 10.7 mg of a white amorphous powder; $[\alpha]_D^{25}$ − 17.60 (*c* 0.27, MeOH); HRESIMS *m/z* 813.4999 $[M-H]^-$, (calculated for $C_{43}H_{73}O_{14}$, 813.5000); for the ^{1}H (pyridine-d_5, 500 MHz) and ^{13}C NMR (pyridine-d_5, 125 MHz) data, see Tables 1 and 3.

2.3.3. *Cyclocarioside Z_{11}* ***(3)***

The separation and purification method afforded 7.4 mg of a white amorphous powder; $[\alpha]_D^{25}$ − 25.27 (*c* 0.23, MeOH); HRESIMS *m/z* 775.4613 $[M+Na]^+$ (calculated for $C_{41}H_{68}O_{12}Na$, 775.4608); for the ^{1}H (pyridine-d_5, 600 MHz) and ^{13}C NMR (pyridine-d_5, 150 MHz) data, see Tables 1 and 3.

2.3.4. *Cyclocarioside Z_{12}* ***(4)***

The separation and purification method afforded 6.2 mg of a white amorphous powder; $[\alpha]_D^{25}$ − 20.47 (*c* 0.19, MeOH); HRESIMS *m/z* 677.3880 $[M+Na]^+$ (calculated for $C_{35}H_{58}O_{11}Na$, 677.3877); for the ^{1}H (pyridine-d_5, 600 MHz) and ^{13}C NMR (pyridine-d_5, 150 MHz) data, see Tables 1 and 3.

2.3.5. *Cyclocarioside Z_{13}* ***(5)***

The separation and purification method afforded 6.2 mg of a white amorphous powder; $[\alpha]_D^{25}$ − 7.26 (*c* 0.31, MeOH); HRESIMS *m/z* 791.4924 $[M+Na]^+$ (calculated for $C_{42}H_{72}O_{12}Na$, 791.4921); for the ^{1}H (pyridine-d_5, 500 MHz) and ^{13}C NMR (pyridine-d_5, 125 MHz) data, see Tables 1 and 3.

Table 3
^{13}C NMR Spectral Data of Compounds 1–11 (125 MHz and 150 MHz, pyridine-d_5, δ in ppm).

Position	Compound **1** δ_C[a]	Compound **2** δ_C[b]	Compound **3** δ_C[a]	Compound **4** δ_C[a]	Compound **5** δ_C[b]	Compound **6** δ_C[b]	Compound **7** δ_C[a]	Compound **8** δ_C[b]	Compound **9** δ_C[b]	Compound **10** δ_C[a]	Compound **11** δ_C[a]
1	35.9	36.0	35.9	36.1	36.0	36.0	35.9	36.0	35.9	36.1	36.0
2	26.1	21.7	21.5	21.8	21.7	21.6	21.6	21.6	21.8	21.6	21.7
3	75.7	79.9	79.5	79.7	79.6	79.6	79.6	79.6	80.0	79.6	80.0
4	39.1	38.2	38.2	38.4	38.3	38.3	38.3	38.3	38.3	38.3	38.2
5	51.2	51.5	51.2	51.4	51.5	51.6	51.3	51.3	51.3	51.3	51.2
6	18.9	18.6	18.6	18.7	18.7	18.7	18.7	18.6	18.6	18.6	18.6
7	37.0	36.7	36.5	36.9	36.7	36.6	36.7	36.7	36.7	36.6	36.6
8	50.6	51.3	50.8	50.5	51.3	51.3	50.9	50.9	50.9	50.4	50.4
9	54.8	54.4	54.2	54.2	54.4	54.4	54.3	54.3	54.3	54.4	54.4
10	40.6	40.3	40.2	40.5	40.3	40.3	40.3	40.3	40.3	40.3	40.3
11	77.0	77.1	77.1	76.6	76.8	76.9	76.8	77.0	76.8	77.3	77.3
12	35.3	34.9	35.0	33.1	35.1	34.9	35.1	34.9	35.1	34.5	34.5
13	41.1	40.9	41.0	41.9	40.8	40.7	40.9	41.0	40.9	41.4	41.4
14	42.0	41.8	41.6	43.3	41.8	41.8	41.8	41.8	41.8	41.8	41.8
15	31.9	31.8	31.5	31.8	31.6	31.6	31.6	31.6	31.6	31.9	31.9
16	27.5	26.1	25.9	27.1	26.0	26.0	25.8	25.9	25.8	27.1	27.1
17	50.5	50.8	50.8	54.3	50.8	50.7	50.7	50.8	50.7	49.6	49.6
18	17.7	17.4	17.3	17.5	17.5	17.5	17.5	17.5	17.5	17.3	17.3
19	17.2	17.0	16.9	16.4	17.0	17.0	16.9	17.1	16.9	17.1	17.1
20	74.4	76.3	74.7	211.3	74.6	74.6	74.4	74.5	74.4	86.8	86.8
21	27.2	27.0	27.6	30.5	27.8	27.9	27.9	27.8	27.8	24.9	24.9
22	38.2	27.0	45.1		45.1	45.0	44.8	44.7	44.8	34.8	34.8
23	31.0	24.8	128.6		76.1	76.1	127.8	127.4	127.7	26.7	26.7
24	76.3	70.3	135.6		127.3	127.4	138.6	138.6	138.6	84.6	84.6
25	150.3	75.0	142.9		135.8	135.8	75.3	75.3	75.3	71.5	71.5
26	110.6	27.7	115.1		18.5	18.6	26.2	26.3	26.3	26.5	26.5
27	19.0	29.2	19.1		26.1	26.1	26.9	26.9	26.9	28.0	28.0
28	23.4	23.2	23.2	23.4	23.3	23.3	23.3	23.3	23.3	23.2	23.2
29	30.5	29.2	30.2	30.4	30.3	30.3	30.3	30.3	30.2	30.3	30.2
30	17.3	17.3	17.0	17.0	17.0	17.2	17.0	17.2	17.1	17.2	17.1
1′		106.8	106.6	106.9	106.8	106.7	106.7	106.7	106.9	106.7	106.9
2′		84.4	84.4	84.6	84.4	84.3	84.4	84.3	84.5	84.4	84.5
3′		80.1	79.7	79.7	79.8	79.8	79.7	79.8	80.2	79.7	80.1
4′		81.8	85.8	86.1	86.0	86.0	86.0	86.1	81.9	85.9	81.8
5′		65.4	63.2	63.4	63.3	63.3	63.3	63.3	65.5	63.3	65.4
1′’	102.1	101.7	102.2	102.0	101.8	102.8	101.9	102.8	101.9	102.1	102.1
2′’	76.2	75.8	75.6	76.0	75.9	73.1	75.9	73.0	75.9	75.7	75.7
3′’	78.7	78.7	78.7	78.8	78.6	75.1	78.6	75.1	78.6	79.0	79.0
4′’	77.3	77.2	78.0	77.3	77.2	70.1	77.2	70.1	77.2	78.1	78.1
5′’	73.2	73.1	72.6	73.1	73.0	67.9	73.0	67.9	73.0	72.8	72.8
6′’	19.1	18.9	63.8	19.1	18.9		19.0		18.9	63.8	63.8
$CH_3\underline{COO}$—		171.1							171.1		171.1
$\underline{CH_3}COO$—		21.0							21.0		21.0
23-$\underline{OCH_3}$					55.5	55.5					
25—$\underline{OCH_3}$							50.5	50.5	50.5		

[a] Recorded at 150 MHz for ^{13}C NMR in pyridine-d_5, chemical shifts given in ppm using TMS as internal reference.
[b] Recorded at 125 MHz for ^{13}C NMR in pyridine-d_5, chemical shifts given in ppm using TMS as internal reference.

2.3.6. *Cyclocarioside Z_{14}* ***(6)***

The separation and purification method afforded 5.0 mg of a white amorphous powder; $[\alpha]_D^{25}$ − 7.76 (*c* 0.19, MeOH); HRESIMS *m/z* 777.4768 $[M+Na]^+$ (calculated for $C_{41}H_{70}O_{12}Na$, 777.4765); for the ^{1}H (pyridine-d_5, 500 MHz) and ^{13}C NMR (pyridine-d_5, 125 MHz) data, see Tables 1 and 3.

2.3.7. *Cyclocarioside Z_{15}* ***(7)***

The separation and purification method afforded 6.6 mg of a white amorphous powder; $[\alpha]_D^{25}$ − 17.75 (*c* 0.25, MeOH); HRESIMS *m/z* 791.4917 $[M+Na]^+$ (calculated for $C_{42}H_{72}O_{12}Na$, 791.4921); for the ^{1}H (pyridine-d_5, 500 MHz) and ^{13}C NMR (pyridine-d_5, 125 MHz) data, see Tables 2 and 3.

2.3.8. *Cyclocarioside Z_{16}* ***(8)***

The separation and purification method afforded 4.1 mg of a white amorphous powder; $[\alpha]_D^{25}$ − 23.51 (*c* 0.30, MeOH); HRESIMS *m/z* 777.4769 $[M+Na]^+$ (calculated for $C_{41}H_{70}O_{12}Na$, 777.4765); for the ^{1}H (pyridine-d_5, 500 MHz) and ^{13}C NMR (pyridine-d_5, 125 MHz) data, see Tables 2 and 3.

2.3.9. *Cyclocarioside Z_{17}* ***(9)***

The separation and purification method afforded 4.7 mg of a white amorphous powder; $[\alpha]_D^{25}$ − 30.61 (*c* 0.22, MeOH); HRESIMS *m/z* 833.5028 $[M+Na]^+$ (calculated for $C_{44}H_{74}O_{13}Na$, 833.5027); for the ^{1}H (pyridine-d_5, 500 MHz) and ^{13}C NMR (pyridine-d_5, 125 MHz) data, see Tables 2 and 3.

2.3.10. *Cyclocarioside Z_{18}* ***(10)***

The separation and purification method afforded 7.1 mg of a white amorphous powder; $[\alpha]_D^{25}$ − 18.42 (*c* 0.25, MeOH); HRESIMS *m/z* 793.4707 $[M+Na]^+$ (calculated for $C_{41}H_{70}O_{13}Na$, 793.4717); for the ^{1}H (pyridine-d_5, 600 MHz) and ^{13}C NMR (pyridine-d_5, 150 MHz) data, see Tables 2 and 3.

2.3.11. *Cyclocarioside Z_{19}* ***(11)***

The separation and purification method afforded 7.5 mg of a white amorphous powder; $[\alpha]_D^{25}$ − 20.47 (*c* 0.22, MeOH); HRESIMS *m/z*

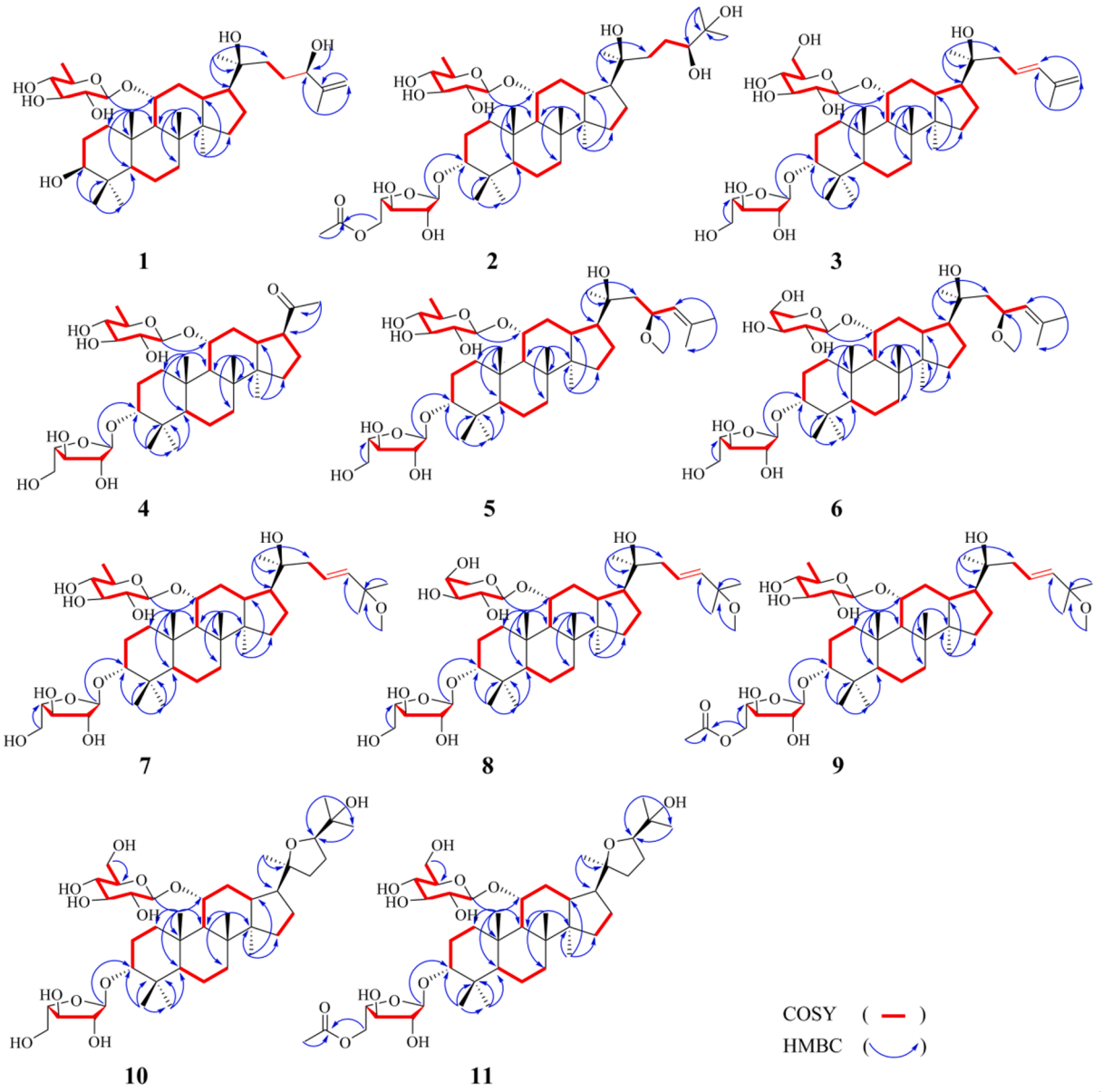

Fig. 2. Key HMBC and COSY correlations of compounds **1**–**11**.

835.4818 $[M+Na]^+$ (calculated for $C_{43}H_{72}O_{14}Na$, 835.4820); for the ^1H (pyridine-d_5, 600 MHz) and ^{13}C NMR (pyridine-d_5, 150 MHz) data, see Tables 2 and 3.

2.4. Hydrolyses of new compounds to determine the linking sugars

The hydrolysis, which was performed according to the previously described method, and HPLC test are shown in the SI (Text S2) [24].

2.5. Assay for the inhibitory effects on α-glucosidase of the fractions and dammarane saponins

The α-glucosidase test was performed according to the previously described PNPG method and is shown in the SI (Text S3) [25].

2.6. Assay for the inhibitory effects on NO production of the extracts and dammarane saponins

The RAW 264.7 cell viability and NO production tests, which were performed according to our previous report, are described in the SI (Text S4) [26,27].

2.7. Reverse transcription-polymerase chain reaction (RT-PCR) assay for active compound **2** on the mRNA expressions of iNOS, COX-2, NF-κB, IL-6, IL-1β and TNF-α

The detailed procedures used by the RT-PCR assay to study the mRNA expression of iNOS, NF-κB, COX-2, IL-6, IL-1β and TNF-α were performed according to a previous report and are described in the SI (Text S5) [28].

2.8. Western blotting assay for active compound 2 on the protein expressions of iNOS, NF-κB/p65 and COX-2

The protein expression of iNOS, NF-κB/p65 and COX-2 was evaluated by performing western blotting according to our previous report, as detailed in the SI (Text S6) [29].

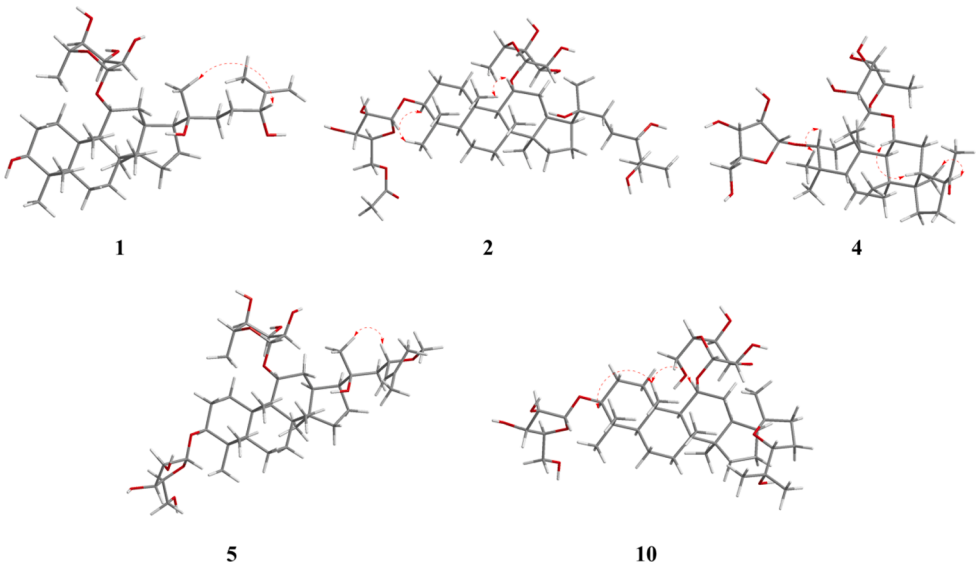

Fig. 3. ROESY correlations of compounds **1**, **2**, **4**, **5**, and **10**.

2.9. Statistical analysis

Each experiment was repeated at least three times in triplicate. The results are expressed as the mean ± SD. The differences were considered statistically significant when (**) $p < 0.01$ or (*) $p < 0.05$.

3. Results and discussion

3.1. Elucidating the structures of the new dammarane saponins

Cyclocarioside **Z9** (**1**) was determined to have the molecular formula $C_{36}H_{62}O_8$ by a positive sodium ion HRESIMS peak at 645.4342 $[M+Na]^+$ (calcd 645.4342 for $C_{36}H_{62}O_8Na$) (Fig. S1). The ^1H NMR data (pyridine-d_5, Table 1) of **1** exhibited eight methyl signals at δ_H 0.87 (s, 30-CH_3), 1.00 (s, 28-CH_3), 1.26 (s, 29-CH_3), 1.91 (s, 27-CH_3), 1.11 (s, 18-CH_3), 1.44 (s, 21-CH_3), 1.40 (s, 19-CH_3), and 1.61 (d, 6′-CH_3); one pair of olefinic protons at δ_H 5.30 (br s, H-26a) and 4.98 (br s, H-26b); and one sugar anomeric proton at δ_H 4.93 (d, $J = 7.6$ Hz, H-1′). The ^{13}C NMR (Fig. S3, pyridine-d_5, Table 1) and DEPT (distortionless enhancement by polarization transfer, pyridine-d_5) data (Fig. S4) of **1** displayed the existence of 36 carbon signals, in which there was one terminal double bond signal at δ_C 150.3 (C-25) and 110.6 (C-26) and one sugar anomeric carbon signal at δ_C 102.1 (C-1′). In the ^1H–^1H COSY (correlation spectroscopy) spectrum of **1**, the correlations of H-1/H-2/H-3, H-5/H-6/H-7, H-9/H-11/H-12/H-13/H-17/H-16/H-15, and H-22/H-23/H-24 substantiated the existence of four fragments of —CH_2CH_2CH—, —$CHCH_2CH_2$—, —$CHCHCH_2CHCHCH_2CH_2$—, and —CH_2CH_2CH— (Figs. 2 and S6). In the HMBC spectrum (Fig. 2 and S7, pyridine-d_5), the cross peaks from H-26 (δ_H 5.30, 4.98, br s) to C-24 (δ_C 76.3) and C-27 (δ_C 19.0) suggested that the terminal double bond (—C═CH_2) was connected to C-25. The HMBC correlations from H-21-CH_3 (δ_H 1.44, s) to C-17 (δ_C 50.5) substantiated that the side chain was located at C-17. The ROESY correlations of H-5/H-9/H-17/H-CH_3-21/H-CH_3-30 suggested that H-5, H-9, H-17, CH_3-21, CH_3-24, and CH_3-30 are α-oriented. The correlations of H-3/H-13/H-CH_3— 18/H-CH_3-19 in the ROESY spectrum indicated that H-3, H-13, H-CH_3-18, and H-CH_3-19 are in the β-orientation (Figs. 3 and S8). Detailed analyses of the abovementioned NMR data showed that the data of **1** was highly similar data to those of 25,26-en-24(*R*)-hydroxyl-20(*S*)-protopanaxadiol, suggesting that **1** includes the basic protopanaxadiol triterpenoid skeleton, differing from 25,26-en-24(*R*)-hydroxyl- 20(*S*)-protopanaxadiol only in the signals at positions 11 and 12 and possessing an extra quinovopyranose (Tables 1 and 3) [30]. The fragment of —CH(9)CH(11)CH_2(12) CH(13)CH(17) CH_2(16)CH_2(15)—, which was confirmed from the ^1H–^1H correlations of **1**, shows that one hydroxyl group was connected at position 11 instead of position 12. Moreover, quinovopyranose was identified in the acid hydrolysis solution of **1** by comparing with the authentic sample by performing a HPLC assay (Table 4). The HMBC correlations between δ_H 4.93 (td, $J = 7.6$ Hz, H-1′) and δ_C 77.0 (C-11) indicated that the quinovopyranosyl group was located at C-11 (Fig. 2). To determine the absolute configuration for chiral centers C-3/11/17/20/24 of **1**, chemical shift comparison for chiral centers (C-3/11/17/20/24) were collected for both *R*- and *S*-enantiomer configurations. For analogous dammaranes, the absolute configurations at C-3/11/17/20 were determined to be *R* with the signals at δ_C 82.4–82.5 (C-3), 76.3 (C-11), 45.0 (C-17), 70.2 (C-20) and be *S* with the signals at δ_C 73.2–73.3 (C-3), 72.8 (C-11), 51.0 (C-17), and 76.2 (C-20) [20,36]. The carbon signals of compound **1** at δ_C 75.7 (C-3), 77.0 (C-11), 50.5 (C-17), 74.4 (C-20) suggested its chiral centers to be 3*S*, 11*R*, 17*S*, and 20*S*. Moreover, 25,26-en-24(*R*)-hydroxyl-20(*S*)-protopanaxadiol and 25,26-en-24(*S*)-hydroxyl-20(*S*)-protopanaxadiol [30], whose structures, together with their absolute configurations, had been identified by analyzing the spectroscopic data as well as chemical methods, have the same chiral centers at C-24 as **1** and could be used as model compounds to assign the absolute configuration of **1** by comparing their C-24 chemical shift values. The ^{13}C NMR datum at δ_C 76.3 (C-24) of **1** more closely resembled that at δ_C 76.4 (C-24) of 25,26-en-24(*R*)-hydroxyl-20(*S*)-protopanaxadiol than that at δ_C 76.0 (C-24) of 25,26-en-24(*S*)-hydroxyl-20

Table 4
The HPLC retention time of sugar moieties of compounds **1**–**11**.

Compounds	Retention times (min)	Types of the monosaccharide
1	8.551	D-Qui
2	7.861, 8.554	L-Ara, D-Qui
3	7.597, 7.844	L-Ara, D-Glc
4	7.840, 8.537	L-Ara, D-Qui
5	7.845, 8.519	L-Ara, D-Qui
6	7.862	L-Ara
7	7.832, 8.498	L-Ara, D-Qui
8	7.876	L-Ara
9	7.833, 8.505	L-Ara, D-Qui
10	7.531, 7.828	L-Ara, D-Glc
11	7.512, 7.824	L-Ara, D-Glc
D-Glc	7.537	
L-Ara	7.843	
D-Qui	8.530	

(*S*)-protopanaxadiol [30]. Consequently, the structure of **1** was deduced as (20*S*,24*R*)-dammarane-24-hydroxyl-11-*O*-*β*-D-quinovopyranosyl and named cyclocarioside **Z$_9$**.

Cyclocarioside **Z$_{10}$** (**2**) was established to have the molecular formula $C_{43}H_{74}O_{14}$ by the negative ion HRESIMS peak at *m/z* 813.4999 $[M-H]^-$ (calcd 813.5000 for $C_{43}H_{73}O_{14}$) (Fig. S9). The ^{1}H NMR data (pyridine-d_5, Table 1, Fig. S10) of **2** showed eight methyl singlets at δ_H 0.76 (s, 30-CH_3), 0.93 (s, 28-CH_3), 1.08 (s, 18-CH_3), 1.24 (s, 29-CH_3), 1.33 (s, 19-CH_3), 1.25 (s, 21-CH_3), 1.29 (s, 27-CH_3), and 1.50 (s, 26-CH_3), a doublet methyl signal at δ_H 1.55 (d, J = 5.9 Hz, 6′′-CH_3) and two glycosyl anomeric protons at δ_H 5.49 (m, H-1′) and 5.03 (d, J = 7.7 Hz, H-1′′). The ^{13}C NMR (pyridine-d_5, Table 3, Fig. S11) and DEPT (distortionless enhancement by polarization transfer, pyridine-d_5) spectra displayed the existence of eight methyl carbon signals at δ_C 17.4 (C-18), 17.0 (C-19), 27.0 (C-21), 27.7 (C-26), 29.2 (C-27), 23.2 (C-28), 29.2 (C-29) and 17.3 (C-30) and two glycosyl anomeric carbon signals δ_C 106.8 (C-1′) and 101.7 (C-1′′). A dammarane-type triterpenoid glycoside structure was established for compound **2**, which is similar to cyclocarioside H, except for the signals of the side chain and connecting position of the glycosyl unit [31]. In the ^{1}H–^{1}H COSY spectrum of **2**, the correlations of H-9/H-11/H-12/H-13/H-17 and H-22/H-23/H-24 substantiated the existence of the two fragments —CHCHCH$_2$CHCH— and —CH$_2$CH$_2$CH— (Figs. 2 and S14). The HMBC peak from H-21-CH_3 (δ_H 1.25, s) to C-17 (δ_C 51.3) suggested that the side chain was connected to C-17. The connections of the two hydroxyl groups at C-24 and C-25 were determined by the key HMBC correlations of H-26 (δ_H 1.50, s) to C-24 (δ_C 70.3), C-25 (δ_C 75.0), C-27 (δ_C 29.2) and H-27 (δ_H 1.29, s) to C-25 (δ_C 75.0) and C-26 (δ_C 27.7). Furthermore, L-arabinose and D-quinovose were identified in the acid hydrolysis solution of **2** by comparing with authentic sugar samples in the HPLC assay (Table 4). The HMBC correlations from the anomeric protons H-1′ (δ_H 5.49, m) to C-3 (δ_C 79.9) and H-1′′ (δ_H 5.03, d) to C-11 (δ_C 77.3) suggested that L-arabinose and D-quinovose were situated at positions 3 and 11, respectively. The HMBC peak from H-5′-CH_3COO— (δ_H 1.96, s) to C-5′ (δ_C 65.5) demonstrated that CH_3COO— was linked to position 5′ (Fig. 2). Moreover, the diagnostic ROESY correlations of H-3/H-11/CH_3-19/CH_3-29 suggested that H-3, H-11, CH_3-19, and CH_3-29 are *β*-oriented. The correlations of H-5/H-9/H-17/H-CH_3— 21/H-CH_3-30 in the ROESY spectrum indicated that H-5, H-9, H-17, CH_3-21, CH_3-24, and CH_3-30 are *α*-oriented (Fig. 3). Moreover, to determine the absolute configuration for chiral centers C-3/11/17/20/24 of **2**, the comparisons of the carbon signals of compound **2** at δ_C 79.9 (C-3), 77.1 (C-11), 50.8 (C-17), 76.3 (C-20) to those of analogous dammaranes indicated its chiral centers to be 3*R*, 11*R*, 17*S*, and 20*S* [20,36]. In addition, the ^{13}C NMR datum at δ_C 70.3 (C-24) of **2** more closely resembled that at δ_C 70.8 (C-24) of 24*R*,25-dihydroxyl protopanaxadiol than that at δ_C 77.1 (C-24) of cyclofoetoside B [32,33]. Thus, compound **2** was deduced as dammarane-(20*S*,24*R*,25)-penthydroxyl-11-*O*-*β*-D-quinovopyranosyl-3-*O*-(5′-*O*-acetyl)-*α*-L-arabinofuranoside and named cyclocarioside **Z$_{10}$**.

Cyclocarioside **Z$_{11}$** (**3**) was determined to have the molecular formula $C_{41}H_{68}O_{12}$ by a positive sodium ion HRESIMS peak at *m/z* 775.4613 $[M+Na]^+$ (calcd 775.4608 for $C_{41}H_{68}O_{12}Na$) (Fig. S17). Detailed analyses of the ^{1}H- and ^{13}C NMR data (pyridine-d_5, Tables 1 and 3) demonstrated that **3** showed features that were closely similar to those of cyclocarioside P, except the quinovopyranosyl moiety was replaced by a glucopyranoside moiety [34]. *α*-L-Arabinopyranose and *β*-D-glucopyranoside were confirmed in the hydrolysate of **3** by comparing with the authentic samples in the HPLC assay (Table 4). The ^{1}H–^{1}H COSY correlations of H-9/H-11/H-12/H-13/H-17 and H-22/H-23/H-24 of **3** demonstrated the presence of the two fragments —CHCHCH$_2$CHCH— and —CH$_2$CHCH— (Figs. 2 and S22). The HMBC correlations from the anomeric protons H-1′ (δ_H 5.52, br s) to C-3 (δ_C 79.5) and H-1′′ (δ_H 5.06, br s) to C-11 (δ_C 77.1) suggested that the two sugar units were situated at positions 3 and 11, respectively (Fig. 2). Furthermore, in the diagnostic ROESY of **3**, the correlations of H-3/H-11/CH_3-19/CH_3-29 indicated that H-3, H-11, CH_3-19, and CH_3-29 are *β*-oriented. The ROESY cross peaks of H-5/H-9/H-17/H-CH_3-21/H-CH_3-30 suggested that H-5, H-9, H-17, CH_3-21, CH_3-24, and CH_3-30 are *α*-oriented (Fig. 3). Furthermore, to determine the absolute configuration for chiral centers C-3/11/17/20 of **3**, the comparisons of the carbon signals of compound **3** at δ_C 79.5 (C-3), 77.1 (C-11), 50.8 (C-17), 74.7 (C-20) to those of analogous dammaranes demonstrated its chiral centers to be 3*R*, 11*R*, 17*S*, and 20*S* [20,36]. Thus, the structure of **3** was deduced as (20*S*,23*E*)-dammarane-11-*O*-*β*-D-glucopyranosyl-3-*O*-*α*-L-arabinofuranoside and named cyclocarioside **Z$_{11}$**.

Cyclocarioside **Z$_{12}$** (**4**) was separated as a white amorphous powder. The molecular formula of $C_{35}H_{58}O_{11}$ of **4** was determined by a positive sodium ion HRESIMS peak at *m/z* 677.3880 $[M+Na]^+$ (calcd 677.3877 for $C_{35}H_{58}O_{11}Na$) (Fig. S25). The ^{1}H- and ^{13}C NMR data of **4** (pyridine-d_5, Tables 1 and 3) were similar to those of cyclocarioside P [34], with the exception of the resonances of the side chain and connecting positions of the glycosyl units, suggesting that **4** also possessed a dammarane-type triterpenoid skeleton. The side chain is cleaved between C-20 and C-22, which is followed by the formation of a keto group at C-20, as confirmed by the HMBC correlations of H-21 (δ_H 2.07) with C-17 (δ_C 54.2) and C-20 (δ_C 211.3). The ^{1}H–^{1}H correlation spectroscopy (COSY) results of H-9/H-11/H-12/H-13/H-17/H-16/H-15 in **4** demonstrated the presence of one —CHCHCH$_2$CHCHCH$_2$CH$_2$— fragment (Figs. 2 and S30). Furthermore, L-arabinose and D-quinovose were confirmed in the acid hydrolysis solution of **4** by comparing with the authentic sugars in the HPLC assay (Table 4). The HMBC correlations from the anomeric protons H-1′ (δ_H 5.56, br s) to C-3 (δ_C 79.7) and H-1′′ (δ_H 4.87, dd) to C-11 (δ_C 76.6) affirmed that the two glycosyl moieties are linked at C-3 and C-11, respectively (Fig. 2). The *β*-orientations of H-3, H-11, H-13, H-CH_3-19, and H-CH_3-29 were then verified by the ROESY peaks of H-13/H-CH_3-18/H-CH_3-19. Similarly, the diagnostic ROESY peaks of H-17 and H-30 demonstrated that H-17 and H-30 are *α*-oriented (Figs. 3 and S32). In addition, to determine the absolute configuration for chiral centers C-3/11/17/20 of **4**, the comparisons of the carbon signals of compound **4** at δ_C 79.7 (C-3), 76.6 (C-11), 50.8 (C-17) to those of analogous dammaranes suggested its chiral centers to be 3*R*, 11*R*, and 17*S* [20,36]. Thus, compound **4** was elucidated as (3*α*,11*α*)-11-*O*-*β*-D-quinovopyranosyl-3-*O*-*α*-L-arabinofuranoside-23,24,25,26,27-hexanor-dammarane-20-one and named cyclocarioside **Z$_{12}$**.

The molecular formula of cyclocarioside **Z$_{13}$** (**5**) was deduced to be $C_{42}H_{72}O_{12}$ due to the positive sodium ion HRESIMS peak at *m/z* 791.4917 $[M+Na]^+$ (calcd 791.4921 for $C_{42}H_{72}O_{12}Na$) (Fig. S33). The ^{1}H NMR data (pyridine-d_5, Table 1) of **5** showed one double bond hydrogen signal at δ_H 5.15 (dt, J = 9.0, 1.3 Hz, 24-H). The detailed analysis of the NMR data showed that **5** was similar to compound **12,** except for the number and positions of the double bonds and the substitution of the methoxy group on the side chain, indicating that **5** also possesses a dammarane skeleton. Compound **5** possessed a double bond between positions 24 and 25 and a methoxy group linking to position 23 in the side chain. L-arabinose and D-quinovose were confirmed in the acid hydrolysis solution of **5** by comparing with the authentic sugars in the HPLC assay (Table 4). The ^{1}H–^{1}H COSY correlations of H-9/H-11/H-12/H-13/H-17/H-16/H-15 and H-22 (δ_H 2.14, m, 1.67, m)/H-23 (δ_H 4.39, m)/H-24 (δ_H 5.15, dt, 9.0, 1.3) demonstrated the presence of the fragments —CHCHCH$_2$CHCHCH$_2$CH$_2$— and —CH$_2$CHCH— (Figs. 2 and S38). The connection of the side chain to position 17 was determined by the key HMBC correlations of δ_H 1.43 (s, H-21) to δ_C 50.8 (C-17), δ_C 74.6 (C-20), and δ_C 45.1 (C-22), those of δ_H 1.69 (s, H-26) to δ_C 127.3 (C-24), δ_C 135.8 (C-25), and δ_C 26.1 (C-27), and the HMBC correlation of δ_H 3.19 (s, 23-OCH_3) to δ_C 76.1 (C-23) (Fig. 2). The diagnostic ROESY correlation of H-23 and H-21 suggested that CH_3-21 and H-23 are *α*-oriented, indicating that the methoxy group at position 23 in the side chain is *β*-oriented (Fig. 3). In addition, compound **5** and cycloarta-24-ene-3*β*,23-diol possess almost the same fragments on the side chain. Considering their ^{13}C NMR data, the ^{13}C NMR data of δ_C 127.3 (C-24) and δ_C 135.8 (C-25) of **5** more closely resembled those of δ_C 128.4 (C-24)

and δ_C 135.6 (C-25) in 23β-cycloarta-24-ene-3β,23-diol than those of δ_C 129.1 (C-24) and δ_C 133.8 (C-25) in 23α-cycloarta-24-ene-3β,23-diol [35]. Moreover, to determine the absolute configuration for chiral centers C-3/11/17/20/23 of **5**, the comparisons of the carbon signals of compound **5** at δ_C 79.6 (C-3), 76.8 (C-11), 50.8 (C-17), 74.6 (C-20) to those of analogous dammaranes demonstrated its chiral centers to be 3*R*, 11*R*, 17*S*, and 20*S* [20,36]. Correspondingly, the absolute configuration of position 23 of **5** was unambiguously confirmed to be *R*. Therefore, the structure of **5** was deduced as (20*S*,23*R*)-dammarane-(3α,11α)-23-methoxy-11-*O*-β-D-quinovopyranosyl-3-*O*-α-L-arabinofuranoside and named cyclocarioside **Z$_{13}$**.

The molecular formula of cyclocarioside **Z$_{14}$** (**6**) was deduced to be $C_{41}H_{70}O_{12}$ due to the positive sodium ion HRESIMS peak at *m/z* 777.4768 $[M+Na]^+$ (calcd 777.4765 for $C_{41}H_{70}O_{12}Na$) (Fig. S41), which is 14 Da less than that of **5**. The ^{1}H- and ^{13}C NMR (pyridine-d_5, Tables 2 and 3) data of **6** are similar to those of **5**, but **6** differed from **5** due to the absence of a methyl group ($-CH_3$) at δ_H 1.60 (d, J = 5.9 Hz). Comparing the ^{1}H- and ^{13}C NMR (Tables 1 and 3) and HRESIMS data between **6** and **5** revealed a significant difference in the data obtained for the sugars and the existence of another arabinose instead of a methyl pentacarbonose in **6**, indicating that **6** also possesses a dammarane skeleton. L-Arabinose was confirmed in the acid hydrolysis solution of **6** by comparing with the authentic sugars in the HPLC assay (Table 4). The arabinopyranoses are linked to positions 3 and 11 in **6**, which was further verified by the key HMBC peaks from the anomeric proton H-1′ (δ_H 5.49, m) to C-3 (δ_C 79.6) and H-1′′ (δ_H 4.81, d) to C-11 (δ_C 76.9) (Fig. 2). In addition, to determine the absolute configuration for chiral centers C-3/11/17/20/23 of **6**, the comparisons of the carbon signals of compound **6** at δ_C 79.6 (C-3), 76.9 (C-11), 50.7 (C-17), 74.6 (C-20) to those of analogous dammaranes indicated its chiral centers to be 3*R*, 11*R*, 17*S*, and 20*S* [20,36]. The absolute configuration of position 23 of **6** was unambiguously confirmed to be *R* by comparing the ^{13}C NMR data of δ_C 127.4 (C-24) and δ_C 135.8 (C-25) of **6** with the ^{13}C NMR data of δ_C 127.3 (C-24) and δ_C 135.8 (C-25) of **5**. Accordingly, the structure of **6** was deduced as (20*S*,23*R*)-dammarane-(3α,11α)-23- methoxy-11-*O*-α-L-arabinopyranosyl-3-*O*-α-L-arabinofuranoside and named cyclocarioside **Z$_{14}$**.

$C_{42}H_{72}O_{12}$ was determined to have the molecular formula cyclocarioside **Z$_{15}$** (**7**) by the positive sodium ion HRESIMS peak at *m/z* 791.4917 $[M+Na]^+$ (calcd 791.4921 for $C_{42}H_{72}O_{12}Na$) (Fig. S49) and possesses the same formula as **5**. Compound **7** had NMR (pyridine-d_5, Tables 2 and 3) signals identical to those of **5**, as revealed by comparing their ^{1}H- and ^{13}C NMR data. The sugar units were confirmed in the acid hydrolysis solution of **5** by comparing with the authentic L-arabinose and D-quinovose in the HPLC assay (Table 4). Small differences between **7** and **5** existed in the ^{1}H- and ^{13}C NMR data (pyridine-d_5) of positions 23, 24, and 25. The ^{1}H NMR data of H-23 and 24 shifted from δ_H 4.39 (m) and 5.15 (dt, 9.0, 1.3) in **5** (pyridine-d_5, Table 1) to δ_H 5.98 (ddd, 15.8, 8.7, 6.2) and 5.65 (d, 15.8) in **7** (pyridine-d_5, Table 2). Moreover, the ^{13}C NMR data of 23, 24, and 25 changed from δ_C 76.1, 127.3, and 135.8 in **5** to δ_C 127.8, 138.6, and 75.3 in **7**, respectively (pyridine-d_5, Table 3). The ^{1}H NMR spectrum of **7** showed a pair of coupled olefinic protons at δ_H 5.98 and 5.65, whose coupling constant of J = 15.8 Hz showed that the configuration of the double bond was *E*. The ^{1}H–^{1}H COSY peaks of H-22 (δ_H 2.61, dd, 13.5, 6.2; δ_H 2.43, dd, 13.5, 8.7)/H-23 (δ_H 5.98, ddd, 15.8, 8.7, 6.2)/H-24 (δ_H 5.65, d, 15.8) of **7** demonstrated the presence of the fragment —CH_2CHCH— (Figs. 2 and S54). In addition, the HMBC correlations from 25-OCH_3 (δ_H 3.20, s) to C-25 (δ_C 75.3) and H-26 (δ_H 1.31, s) to C-24 (δ_C 138.6), C-25 (δ_C 75.3) and C-27 (δ_C 26.9) (Fig. 2) indicated that the methoxy group is linked to position 25. Furthermore, to determine the absolute configuration for chiral centers C-3/11/17/20 of **7**, the comparisons of the carbon signals of compound **7** at δ_C 79.6 (C-3), 76.8 (C-11), 50.7 (C-17), 74.4 (C-20) to those of analogous dammaranes indicated its chiral centers to be 3*R*, 11*R*, 17*S*, and 20*S* [20,36]. Therefore, the structure of **7** was deduced as (23*E*,20*S*)-dammarane(3α,11α)-25-hydroxyl-11-*O*-β-D-quinovopyranosyl-3-*O*-α-L-arabinofuranoside and named cyclocarioside **Z$_{15}$**.

The molecular formula of cyclocarioside **Z$_{16}$** (**8**) was determined to be $C_{41}H_{70}O_{12}$ by the positive sodium ion HRESIMS peak at *m/z* 777.4769 $[M+Na]^+$ (calcd 777.4765 for $C_{41}H_{70}O_{12}Na$) (Fig. S57), which is 14 Da less than that of **7**. The detailed analysis of the ^{1}H- and ^{13}C NMR (pyridine-d_5, Tables 2 and 3) data showed that **8** was very similar to **7,** except the quinovopyranosyl moiety was replaced by an arabinopyranosyl moiety at C-11 in **8**. Moreover, the hydrolysate of compound **8** obtains L-arabinose, which was determined by comparing with the authentic sample in the HPLC test (Table 4). Accordingly, the structure of **8** was deduced as (23*E*,20*S*)-dammarane-(3α,11α)-25-hydroxyl-11-*O*-α-L-arabinopyranosyl-3-*O*-α-L-arabinofuranoside and named cyclocarioside **Z$_{16}$**.

The molecular formula of cyclocarioside **Z$_{17}$** (**9**) was determined to be $C_{44}H_{74}O_{13}$ by the positive sodium ion HRESIMS peak at *m/z* 833.5028 $[M+Na]^+$ (calcd 833.5027 for $C_{44}H_{74}O_{13}Na$) (Fig. S65), which is 42 Da more than that of **7**. Detailed comparisons of the ^{1}H- and ^{13}C NMR (pyridine-d_5, Tables 2 and 3) data showed that **9** was highly analogous to **7,** except for the replacement of an acetyl moiety (CH_3CO—) at C-5′ of L-arabinose linked to C-3 in **9**, which was confirmed by the HMBC correlations of H-5′ (δ_H 4.81, dd, 11.6, 3.0; δ_H 4.62, m) with C=O ($CH_3\underline{C}O$—, δ_C 171.1) (Fig. 2). Besides, the glycosyl moieties were determined by acid hydrolysis and HPLC analysis with L-arabinose and D-quinovose standard (Table 4). Accordingly, the structure of **8** was deduced as (23*E*,20*S*)-dammarane-(3α,11α)-25-hydroxyl-11-*O*-α-L-arabinopyranosyl-3-*O*-α-L-arabinofuranoside and named cyclocarioside **Z$_{16}$**.

Cyclocarioside **Z$_{18}$** (**10**) yielded a positive sodium ion HRESIMS peak at *m/z* 793.4717 $[M+Na]^+$ (calcd 793.4707 for $C_{41}H_{70}O_{13}Na$) (Fig. S73), which revealed the molecular formula of $C_{41}H_{70}O_{13}$. Comparing the ^{1}H- and ^{13}C NMR data (pyridine-d_5, Tables 2 and 3) of **10** with those of the related compounds in the literature indicated that the data of **10** were highly similar to those of cyclocarioside I, [34] except for the signals replacing D-glucopyranose with D-quinovose and the connecting position of D-glucopyranose (pyridine-d_5, Tables 2 and 3). The ^{1}H–^{1}H COSY correlations of H-9/H-11/H-12/H-13 of **10** demonstrated the presence of the fragment —CHCHCH_2CH— (Figs. 2 and S78). Furthermore, the diagnostic ROESY correlations of H-3 and H-11 to H-19 suggested that H-3, H-11 and H-19 are β-oriented. Similarly, the diagnostic ROESY peaks of H-17 and H-30 indicated that H-17 and H-30 are α-oriented (Fig. 3). In addition, α-L-arabinopyranose and β-D-glucopyranose were confirmed by the hydrolysis and HPLC test (Table 4). The HMBC correlations from the anomeric proton δ_H 5.53 (br s, H-1′) to δ_C 79.6 (C-3) and δ_H 5.16 (d, H-1′′) to δ_C 77.3 (C-11) suggested that α-L-arabinopyranose and β-D-glucopyranoside are connected to C-3 and C-11, respectively (Fig. 2). In addition, to determine the absolute configuration for chiral centers C-3/11/17/20/24 of **10**, the comparisons of the carbon signals of compound **10** at δ_C 79.6 (C-3), 77.3 (C-11), 49.6 (C-17), 86.8 (C-20), 84.6 (C-24) to those of analogous dammaranes demonstrated its chiral centers to be 3*R*, 11*R*, 17*S*, 20*S*, and 24*S* [20,36]. Finally, the structure of **10** was deduced as (20*S*,24*R*)-epoxydammara-(3α,11α)-25-hydroxyl-11-*O*-β-D-glucopyranoside-3-*O*-α-L-arabinofuranoside, and **10** was named cyclocarioside **Z$_{18}$**.

Cyclocarioside **Z$_{19}$** (**11**) yielded a positive sodium ion HRESIMS peak at *m/z* 835.4818 $[M+Na]^+$ (calcd 835.4820 for $C_{43}H_{72}O_{14}Na$) (Fig. S81), demonstrated a molecular formula of $C_{43}H_{72}O_{14}$ and is 42 Da more than that of **10**. Analysis of the ^{1}H- and ^{13}C NMR (pyridine-d_5, Tables 2 and 3) data showed that **11** was analogous to **10,** except for the replacement of an acetyl group at C-5′ of L-arabinose linking to C-3 in **11**, which was confirmed by the HMBC correlations of H-5′ (δ_H 4.81, dd, 11.5, 3.0; δ_H 4.61 m) with C=O ($CH_3\underline{C}O$—, δ_C 171.1) (Fig. 2). In addition, α-L-arabinopyranose and β-D-glucopyranose were confirmed by acid hydrolysis and HPLC analysis (Table 4). Therefore, the structure of **11** was deduced as (20*S*,24*R*)-epoxydammarane-(3α,11α)-25-hydroxyl-11-*O*-β-D-glucopyranoside-3-*O*-(5′-*O*-acetyl)-α-L-arabinofuranoside and

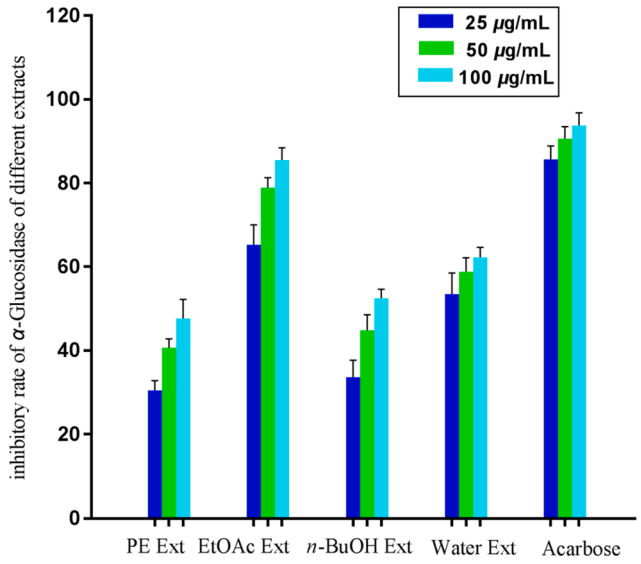

Fig. 4. Inhibitory effects against α-glucosidase of the different fractions.

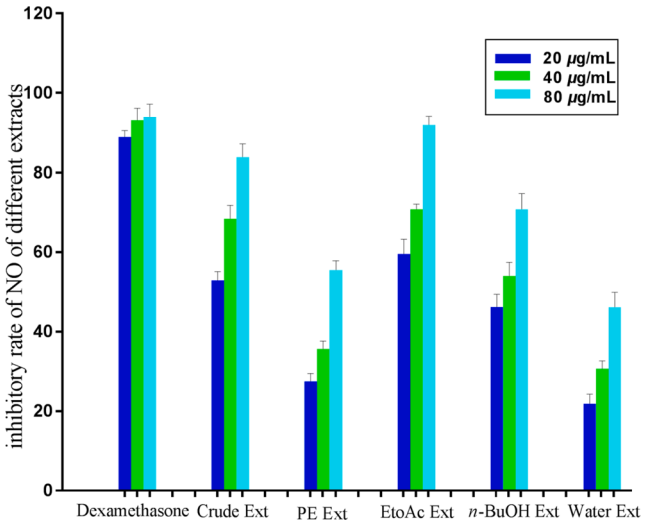

Fig. 5. Inhibitory effects against NO of the different fractions in LPS-mediated RAW 264.7 cells.

Table 5
Inhibitory activities on α-Glucosidase of Compounds **1**-**20**.[a]

Compounds	IC_{50} (μmol)	Compounds	IC_{50} (μmol)
1	282.23 ± 1.84	**12**	274.77 ± 1.13
2	257.74 ± 1.55	**13**	287.71 ± 1.08
3	290.84 ± 0.99	**14**	306.99 ± 0.79
4	578.77 ± 0.94	**15**	383.50 ± 0.82
5	330.29 ± 1.17	**16**	>500
6	369.54 ± 0.71	**17**	>500
7	447.72 ± 0.62	**18**	478.15 ± 1.44
8	>500	**19**	>500
9	451.22 ± 1.63	**20**	/
10	>500	acarbose [b]	359.36 ± 0.65
11	>500		

[a] All values are means of three independent experiments.
[b] Acarbose, a hypoglycemic drug used as positive control.

Table 6
Inhibitory Activities on NO of Compounds **1**–**20** in LPS-induced RAW 264.7 Cell [a]

Compounds	IC_{50} (μM)	Compounds	IC_{50} (μM)
1	9.10 ± 0.11	**12**	>40
2	9.02 ± 0.14	**13**	30.76 ± 0.43
3	>40	**14**	23.74 ± 0.12
4	>40	**15**	24.18 ± 0.66
5	13.94 ± 0.17	**16**	30.19 ± 0.17
6	12.57 ± 0.41	**17**	>40
7	16.41 ± 0.12	**18**	23.17 ± 0.57
8	15.42 ± 0.75	**19**	30.44 ± 0.19
9	15.86 ± 0.44	**20**	/
10	26.47 ± 0.78	Dexamethasone [b]	9.17 ± 0.41
11	27.19 ± 0.51		

[a] All values are means of three independent experiments.
[b] Dexamethasone, an anti-inflammatory agent used as positive control.

named cyclocarioside $\mathbf{Z_{19}}$.

By comparing the NMR (^{1}H and ^{13}C) and MS data to those reported in the literature, the known dammarane saponins were identified as cyclocarioside P (**12**) [34], cyclocarioside O (**13**) [34], cyclocarioside L (**14**) [36], cyclocarioside M (**15**) [36], cyclocarioside H (**16**) [34], cyclocarioside B (**17**) [37], cyclocarioside J (**18**) [37], cyclocarioside I (**19**) [14], and octyl ursolate (**20**) [38].

3.2. The extracts and dammarane saponins inhibit the activity of α-glucosidase

The inhibitory activities towards α-glucosidase of the PE, EtOAc, *n*-butanol, and H_2O fractions obtained from the 75% EtOH/H_2O extract are shown in Fig. 4. The results show that the EtOAc fraction (Fr. EtOAc) obtained from the 75% EtOH/H_2O extract strongly inhibited α-glucosidase, in a manner comparable to the inhibition effect of the positive control acarbose.

The inhibitory effects of dammarane saponins **1**–**20** isolated from the active EtOAc fraction on α-glucosidase are shown in Table 5. Dammarane saponins **1**–**3**, **5**, and **12**–**14** showed a strong inhibitory activity against α-glucosidase, with IC_{50} values ranging from 257.74 μM to 290.84 μM. These values are superior to those of the positive control, acarbose (359.36 μM). Dammarane saponin **2** revealed the strongest inhibitory activity against α-glucosidase, with an IC_{50} value of 257.74 μM. Dammarane saponins **6** and **15** had good effects, with IC_{50} values of 369.54 μM and 383.50 μM, respectively, which are equal to the IC_{50} values of the positive control acarbose. Dammarane saponins **4**, **7**, **9**, and **18** had moderate effects, with IC_{50} values ranging from 451.22 μM to 478.15 μM. Dammarane saponins **8**, **10**–**11**, **16**–**17** and **19**–**20** exhibited no inhibition against α-glucosidase. The results showed that there are abundant dammarane saponins in *C. paliurus* eaves, showing α-glucosidase inhibition.

3.3. The extracts and dammarane saponins reduce the production of NO in LPS-mediated RAW 264.7 cells

The RAW 264.7 cell viability assay showed that the extracts and all of the dammarane saponins were not cytotoxic at a concentration of 40 μM, and the cells had a survival rate up to 90%.

The inhibitory effects on NO production of the 75% EtOH/H_2O extract (crude Ext) and the PE fraction (Fr. PE), Fr. EtOAc, Fr. *n*-butanol, and Fr·H_2O from the crude Ext are shown in Fig. 5. Fr. EtOAc strongly inhibited the production of NO in LPS-mediated RAW 264.7 cells and exhibited an inhibitory effect equal to that of dexamethasone (positive control). The active anti-inflammatory Fr. EtOAc was further isolated to obtain 20 dammarane saponins. The inhibitory effects of dammarane saponins **1**–**20** against LPS-mediated NO production in RAW 264.7 cells are listed in Table 6. The results show that dammarane saponins **1** and **2** strongly suppressed NO production, with IC_{50} values of 9.10 μM and 9.02 μM, respectively, and **1** and **2** were better than dexamethasone, with an IC_{50} value of 9.17 μM. Dammarane saponins **5**–**9** had moderate effects on inhibiting NO production, with IC_{50} values ranging from

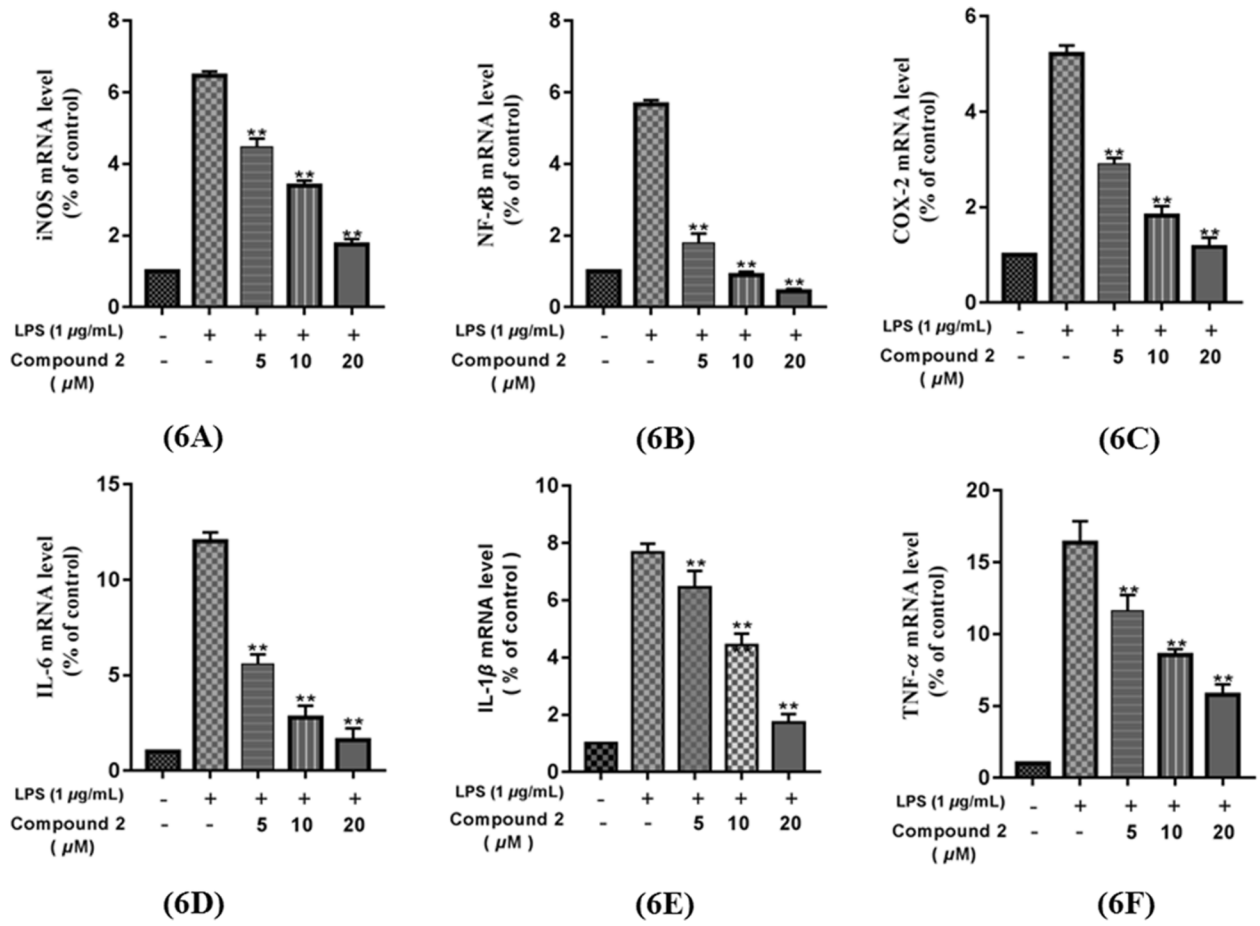

Fig. 6. Effect of compound **2** on LPS-mediated mRNA expression of IL-6, IL-1β, iNOS, NF-κB, COX-2 and TNF-α. RAW264.7 cells were pre-incubated with various concentrations of compound **2** (5, 10 and 20 μM) for 1 h followed by stimulation with LPS (1 μg/mL) for 24 h. The mRNA expression of iNOS (6**A**), NF-κB (6**B**), COX-2 (6**C**), IL-6 (6**D**), IL-1β (6**E**) and TNF-α (6**F**) was analyzed using Real-time RT-PCR. The data are presented as mean ± SDs (n = 3), **p < 0.01 represent significance when compared to LPS-only treated cells.

12.57 μM to 16.41 μM. Dammarane saponins **10**–**11**, **13**–**16** and **18**–**19** inhibited NO production, with IC_{50} values ranging from 23.17 μM to 30.76 μM. Dammarane saponins **3**–**4**, **12**, **17** and **20** did not inhibit NO production, with IC_{50} values above 40 μM. The results demonstrated that there are abundant dammarane saponins in *C. paliurus* leaves that inhibit NO production.

Although dammarane saponin **1** has a hydroxyl group linked to position 3, all other dammarane saponins, **2**–**20**, have arabinose or its derivatives linked to position 3. The differences between these compounds are mainly in the sugars linked to position 11 and the changes in the side chains. Comparing the structures of these dammarane saponins with their inhibitory activities towards α-glucosidase and NO production revealed that the number of hydroxyl groups in the isolate side chains affects their inhibitory activity. Dammarane saponins **1** and **2**, which have many hydroxyl groups in their side chains, showed a better activity than the compounds with fewer hydroxyl groups. Moreover, an epoxy ring on the side chain seemed to be related to α-glucosidase and NO production potency. For example, the inhibition of α-glucosidase and NO production of **1**, **2**, **5**, **6**, **7**, **12**, and **13** with no ring in the side chain were greater than those of **10**, **11**, **16**, **17**, and **19** with epoxy rings on the side chains. Furthermore, the kinds of glycosyl units significantly influenced the inhibitory effects on α-glucosidase and NO production. Dammarane saponins **6**, **8**, **13**, and **18**, with an arabinopyranosyl unit at position 11, more strongly inhibited NO production than their corresponding dammarane saponins **5**, **7**, **12**, and **17** with a quinovopyranosyl unit at position 11. In addition, the inhibition of NO production seems to be related to whether there is a full side chain at position 17. For example, **4**, which has a side chain that is cleaved between C-20 and C-22, showed a lower inhibitory activity against α-glucosidase than dammarane saponins **5**–**9** and **13**–**16** and exhibited no activity against NO production. In addition, compounds with many double bonds on the side chains more weakly inhibited NO production than did compounds with few double bonds. For example, **3**, **12**, and **13** with two double bonds on the side chains exhibited weak or no activity against NO production. In summary, the α-glucosidase inhibitory and anti-inflammatory activities of these dammarane saponins are related to the kind of glycosyl unit substituted at position 11, the number of hydroxyl groups, the epoxy ring, the cleavage of the side chain, and the number of double bonds on the side chain.

3.4. Active dammarane saponin 2 inhibits the mRNA expression of iNOS, COX-2, NF-κB, IL-6, IL-1β and TNF-α

LPS alone markedly increased the mRNA expression of iNOS (Fig. 6A), NF-κB (Fig. 6B), COX-2 (Fig. 6C), IL-6 (Fig. 6D), IL-1β (Fig. 6E) and TNF-α (Fig. 6F) in LPS-mediated RAW 264.7 cells, as shown in Fig. 6. However, secretions of these inflammatory cytokines all decreased after pretreatment with compound **2** at concentrations of 20, 10, and 5 μM. Generally, the results suggested that compound **2** can inhibit the mRNA expression of iNOS, NF-κB, COX-2, IL-6, IL-1β and TNF-α in a concentration-dependent manner in LPS-mediated RAW 264.7 cells.

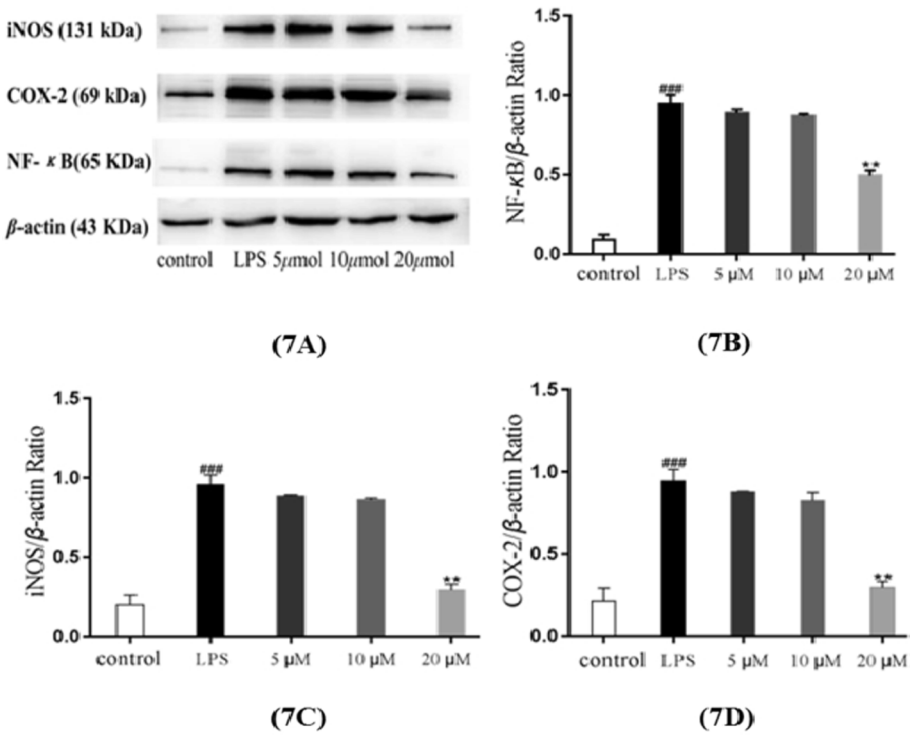

Fig. 7. Effects of compound **2** at concentrations of 5, 10, and 20 μM on iNOS, COX-2, and NF-κB/p65 expression in LPS-mediated RAW 264.7 cells. β-Actin served as the loading control. ** $p < 0.01$ compared with cells treated with LPS, $^{###}p < 0.001$ compared with control that was activated without LPS.

3.5. Active dammarane saponin 2 inhibits the protein expression of iNOS, NF-κB/p65 and COX-2

Mediated by LPS, the protein expression levels of iNOS, NF-κB/p65, and COX-2 were significantly higher than the levels of the control cells (Fig. 7). After treatment with **2**, the protein expression levels of iNOS, NF-κB/p65, and COX-2 were significantly suppressed. Compound **2** inhibited the protein expression levels of iNOS, NF-κB/p65, and COX-2 in LPS-mediated RAW 264.7 cells in a dose-dependent manner.

4. Conclusions

Diabetes mellitus is caused by chronic inflammation and affects millions of people worldwide. *C. paliurus* leaves have been widely used in traditional folk tea as a remedy for diabetes. An extract of *C. paliurus* leaves showed significantly reduced blood glucose, an improved glucose tolerance, and attenuated damage to pancreatic islets. However, the possible antidiabetic constituents and mechanisms remain unclear. The α-glucosidase inhibitory- and anti-inflammatory-guided separation of the *C. paliurus* leaves led to the identification of 20 dammarane saponins, including eleven new dammarane saponins (**1**–**11**). Bioassays demonstrated that dammarane saponins **1**–**3**, **5**, and **12**–**14** showed potent inhibitory effects against α-glucosidase and NO production in LPS-mediated RAW 264.7 cells. The most active compound (**2**) significantly downregulated the mRNA expression of iNOS, COX-2, IL-1β, NF-κB, IL-6 and TNF-α and markedly suppressed the protein expression of iNOS, NF-κB/p65, and COX-2 in LPS-mediated RAW 264.7 cells, suggesting that compound **2** produced α-glucosidase inhibitory and anti-inflammatory activities by inhibiting NF-κB signaling pathways. Dammarane glucoside **2** exhibited the strongest α-glucosidase inhibitory and anti-inflammatory activities. In addition, the structure–activity relationship analysis indicated that the α-glucosidase inhibitory and anti-inflammatory activities of these dammarane saponins are related to the kind of glycosyl unit substituted at position 11, the number of hydroxyl groups, the epoxy ring, the cleavage of the side chain, and the number of double bonds in the side chain. These findings demonstrated that *C. paliurus* leaves contain abundant dammarane saponins with α-glucosidase inhibitory and anti-inflammatory activities, which could be meaningful for discovering new antidiabetic agents.

Declaration of Competing Interest

The authors declare that they have no known competing financial interests or personal relationships that could have appeared to influence the work reported in this paper.

Acknowledgments

Authors (J. Li. and X. S. Huang) acknowledge the following grants for funding this project: National Natural Science Foundation of China (32060097); The Natural Science Fund of Guangxi Province (2018GXNSFDA050007, 2018GXNSFAA050042, and 2018GXNSFAA281102); The Open Research Fund program of the Key Laboratory for the Chemistry and Molecular Engineering of Medicinal Resources (CMEMR2020-A04); The Fund of Guilin Scientific Research and Technology Development Program (20190205).

Appendix A. Supplementary material

Supplementary data to this article can be found online at https://doi.org/10.1016/j.bioorg.2021.104847.

References

[1] A.E. Al-Snafi, W.J. Majid, T.A. Talab, H.A. Al-Battat, Medicinal plants with antidiabetic effects – an overview (Part 1), IOSR J. Pharm. 9 (2019) 9–46.
[2] N.G. Joy, D.B. Tate, L.M. Younk, S.N. Davis, Effects of acute and antecedent hypoglycemia on endothelial function and markers of atherothrombotic balance in healthy humans, Diabetes 64 (2015) 2571–2580.
[3] F.S. Atkinson, K. Foster-Powell, J.C. Brand-Miller, International tables of glycemic index and glycemic load values: 2008, Diabetes Care 31 (2008) 2281–2283.

[4] T. Fujisawa, H. Ikegami, K. Inoue, Y. Kawabata, T. Ogihara, Effect of two alpha-glucosidase inhibitors, voglibose and acarbose, on postprandial hyperglycemia correlates with subjective abdominal symptoms, Metabolism 54 (2005) 387–390.

[5] H. Yin, W.J. Dan, B.Y. Fan, C. Guo, K. Wang, D. Li, K.F. Xian, G. Pescitelli, J.M. Gao, Anti-inflammatory and α-glucosidase inhibitory activities of labdane and norlabdane diterpenoids from the rhizomes of *Amomum villosum*, J. Nat. Prod. 82 (2019) 2963–2971.

[6] B.B. Duncan, M.I. Schmidt, J.S. Pankow, C.M. Ballantyne, D. Couper, A. Vigo, R. Hoogeveen, A.R. Folsom, G. Heiss, Low-grade systemic inflammation and the development of type 2 diabetes: the atherosclerosis risk in communities study, Diabetes 52 (2003) 1799–1805.

[7] X.T. Zhai, Z.Y. Zhang, C.H. Jiang, J.Q. Chen, J.Q. Ye, X.B. Jia, Y. Yang, Q. Ni, S. X. Wang, J. Song, F.X. Zhu, Nauclea officinalis inhibits inflammation in LPS-mediated RAW 264.7 macrophages by suppressing the NF-κB signaling pathway, J. Ethnopharmacol. 183 (2016) 159–165.

[8] Z. Liu, Y. Fan, Y. Wang, C. Han, Y. Pan, H. Huang, Y. Ye, L. Luo, Z.M. Yin, Dipyrithione inhibits lipopolysaccharide-induced iNOS and COX-2 up-regulation in macrophages and protects against endotoxic shock in mice, FEBS Lett. 582 (2008) 1643–1650.

[9] M. Dorenkamp, A. Riad, S. Stiehl, F. Spillmann, D. Westermann, J. Du, M. Pauschinger, M. Noutsias, V. Adams, H.P. Schultheiss, Protection against oxidative stress in diabetic rats: role of angiotensin AT1 receptor and beta 1-adrenoceptor antagonism, Eur. J. Pharmacol. 520 (2005) 179–187.

[10] S. Alizadeh, H. Mazloom, A. Sadeghi, S. Emamgholipour, A. Golestani, F. Noorbakhsh, M. Khoshniatnikoo, R. Meshkani, Evidence for the link between defective autophagy and inflammation in peripheral blood mononuclear cells of type 2 diabetic patients, J. Physiol. Biochem. 74 (2018) 369–379.

[11] H.M. Peng, X.J. He, J.X. Chen, Y.Q. Qu, F.R. Zhang, W.B. Wu, Y.J. Zeng, Hypoglycemic effects of extracts of *Cyclocarya paliurus* (Batal.) Ijinskaja for experimental diabetic model mice, J. Sichuan. Trad. Chinese Med. 36 (2018) 60–63.

[12] L.C. Zhao, X. Wang, J.X. Li, X.M. Tan, L.L. Fan, Z.W. Zhang, J. Leng, Effect of *Cyclocarya Paliurus* on hypoglycemic effect in type 2 diabetic mice, Med. Sci. Monitor 25 (2019) 2976–2983.

[13] D.J. Yang, Z.C. Zhong, Z.M. Xie, Studies on the sweet principles from the leaves of *Cyclocarya paliurus* (Batal.), Iljinsk. Acta Pharm. Sin. 27 (1992) 841–844.

[14] R.G. Shu, C.R. Xu, L.N. Li, Sweet principles from the leaves of *Cyclocarya paliurus* (Batal.) Iljinsk, Acta Pharm. Sin. 30 (1995) 757–761.

[15] C.H. Jiang, Y.T. Wang, Q.M. Jin, D.J. Zhang, M. Gao, N. Yao, Z.Q. Yin, J. Zhang, S. P. Ma, Cyclocarya paliurus triterpenoids improve diabetes-induced hepatic inflammation via the Rho-kinase-dependent pathway, Front Pharmacol. 10 (2019) 811/1–811/13.

[16] J. Li, W.W. Zeng, Y.X. Wu, Q. Zhang, M. Luo, Y.H. Zhu, X.L. Yang, A.Y. Guo, Integrating transcriptome and experiments reveals the antidiabetic mechanism of *Cyclocarya paliurus* formula, Mol. Ther. Nucl. Acids. 13 (2018) 419–430.

[17] J. Li, X.L. Yang, Y.H. Zhu, M. Luo, A.Y. Guo, Q. Zhang, Investigating the molecular mechanism of aqueous extract of Cyclocarya paliurus on ameliorating diabetes by transcriptome profiling, Front Pharmacol. 9 (2018), 912-912.

[18] Y. Liu, Y.N. Cao, S.Z. Fang, T.L. Wang, Z.Q. Yin, X.L. Shang, M.H. Hu, Antidiabetic effect of *Cyclocarya paliurus* leaves depends on the contents of antihyperglycemic flavonoids and antihyperlipidemic triterpenoids, Molecules 23 (2018) 1042.

[19] L.X. Zhai, Z.W. Ning, T. Huang, B. Wen, C.H. Liao, C.Y. Lin, L. Zhao, H.T. Xiao, Z. X. Bian, Cyclocarya paliurus leaves tea improves dyslipidemia in diabetic mice: a lipidomics-based network pharmacology study, Front Pharmacol. 9 (2018), 973-973.

[20] H.H. Sun, J. Tan, W.Y. Lv, J. Li, J.P. Wu, J.L. Xu, H. Zhu, Z.C. Yang, W.X. Wang, Z. X. Zou, Z.H. Chen, K.P. Xu, Hypoglycemic triterpenoid glycosides from Cyclocarya paliurus (sweet tea tree), Bioorg. Chem. 95 (2020) 103493/1–103493/8.

[21] X.M. Jiang, Q.X. Lin, G.D. He, X.H. Hou, Z.X. Shan, Y.M. Du, Therapeutic effect of QQL prescription on type 2 diabetic rats, Chin. J. Pathophysiol. 33 (2017) 1794–1800.

[22] Z.W. Ning, L.X. Zhai, T. Huang, J. Peng, D. Hu, H.T. Xiao, B. Wen, C.Y. Lin, L. Zhao, Z.X. Bian, Identification of alpha-glucosidase inhibitors from *cyclocarya paliurus* tea leaves using UF-UPLC-Q/TOF-MS/MS and molecular docking, Food Funct. 10 (2019) 1893–1902.

[23] J.K. Yao, J.X. Wang, X.M. Gao, L. Fu, F. Gao, Y.J. Wang, Effects of *Cyclocarya Paliurus* leaves aqueous extract on pancreatic β cell's apoptosis in type 2 diabetic rats, J. Beijing U. Trad. Chin. Med. 41 (2018) 663–669.

[24] L. Lindqvist, P.E. Jansson, Determination of the absolute configuration of sugar residues using gas chromatography - method with potential for elimination of references, J. Chromatogra. A 769 (1997) 253.

[25] M. Emre, B. Nimet, M. Emirik, Synthesis, α-glucosidase inhibition and in silico studies of some 4-(5-fluoro-2-substituted-1H-benzimidazol-6-yl)morpholine derivatives, Bioorg. Chem. 101 (2020) 104002.

[26] T. Jayakumar, H.C. Huang, C.W. Hsia, T.H. Fong, K. Themmila, V. Marappan, M. Manjunath, J.R. Sheu, C.H. Hsia, Ruthenium derivatives attenuate LPS-induced inflammatory responses and liver injury via suppressing NF-κB signaling and free radical production, Bioorg. Chem. 96 (2020) 103639.

[27] P.P. Guan, X.B. Wang, Y. Jiang, N.N. Dou, X.D. Qu, J. Liu, B. Lin, L. Han, X. S. Huang, C.L. Jiang, The anti-inflammatory effects of jiangrines from *Jiangella alba* through inhibition of p38 and NF-κB signaling pathways, Bioorg. Chem. 95 (2020) 103507.

[28] P.J. Jacob, S.L. Manju, Identification and development of thiazole leads as COX-2/5-LOX inhibitors through in-vitro, and in-vivo, biological evaluation for anti-inflammatory activity, Bioorg. Chem. 100 (2020) 103882.

[29] Y. Zhang, J. Liu, M. Wang, C. Sun, X. Li, Five new compounds from *Hosta plantaginea* flowers and their anti-inflammatory activities, Bioorg. Chem. 95 (2020) 103494.

[30] G.T. Chen, X. Yang, J.L. Li, H.J. Ge, Y. Song, J. Ren, Biotransformation of 20(*S*)-protopanaxadiol by *Aspergillus niger* AS 3.1858, Fitoterapia 91 (2013) 256–260.

[31] S. Li, B.S. Cui, Q. Liu, L. Tang, Y.C. Yang, X.J. Jin, Z.F. Shen, New triterpenoids from the leaves of *Cyclocarya paliurus*, Planta Med. 78 (2012) 290–296.

[32] G.J. Du, Q. Dai, S. Williams, C.Z. Wang, C.S. Yuan, Synthesis of protopanaxadiol derivatives and evaluation of their anticancer activities, Anticancer Drugs 22 (2011) 35–45.

[33] T.V. Ganenko, M.I. Isaev, T.T. Gorovits, A.S. Gromova, V.I. Lutskii, A.A. Semenov, M.B. Gorovits, N.K. Abubakirov, Triterpene glycosides and their genins from *Thalictrum foetidum* V structure of cyclofoetoside B, Chem. Nat. Compd. 22 (1986) 315–319.

[34] Y.R. Wang, B.S. Cui, S.W. Han, S. Li, New dammarane triterpenoid saponins from the leaves of *Cyclocarya paliurus*, J. Asian Nat. Prod. Res. 20 (2018) 1019–1027.

[35] H.G. Lago, C.B. Brochini, N.F. Roque, Terpenoids from *Guarea guidonia*, Phytochemistry 60 (2002) 333–338.

[36] Z.F. Wu, F.C. Meng, L.J. Cao, C.H. Jiang, M.G. Zhao, X.L. Shang, S.Z. Fang, W.C. Ye, Q.W. Zhang, J. Zhang, Z.Q. Yin, Triterpenoids from *Cyclocarya paliurus* and their inhibitory effect on the secretion of apoliprotein B48 in Caco-2 cells, Phytochemistry 142 (2017) 76–84.

[37] Z.Y. Jiang, X.M. Zhang, J. Zhou, S.X. Qiu, J.J. Chen, Two new triterpenoid glycosides from *Cyclocarya paliurus*, J. Asian Nat. Prod. Res. 8 (2006) 93–108.

[38] Y.J. Liu, J.L. Xie, Ursolate compounds from fruit of *Diospyros kaki L f*, J. Plant Res. Environ. 10 (2001) 1–3.